

CZECH TECHNICAL UNIVERSITY IN PRAGUE

FACULTY OF MECHANICAL ENGINEERING

**DEPARTMENT OF MECHANICS, BIOMECHANICS AND
MECHATRONICS**

**MUSCLE ACTIVITY DRIVEN BY
PROPRIOCEPTION**

by Bc. et Bc. Jiří Bešťák

supervisor prof. RNDr. Matej Daniel, Ph.D

Prague, 2023



MASTER'S THESIS ASSIGNMENT

I. Personal and study details

Student's name: **Bešťák Jiří** Personal ID number: **482798**
Faculty / Institute: **Faculty of Mechanical Engineering**
Department / Institute: **Division of biomechanics**
Study program: **Applied Sciences in Mechanical Engineering**
Specialisation: **Biomechanics**

II. Master's thesis details

Master's thesis title in English:

Muscle activity driven by proprioception

Master's thesis title in Czech:

Řízení svalové aktivity na základě propriocepce

Guidelines:

1. Proprioception in biomechanics - state of the art
2. Musculoskeletal model of a selected joint
3. Solution of the muscle redundancy problem using optimization methods
4. Implementation of proprioception into the musculoskeletal model
5. Design of optimization criterion using proprioception
6. Prediction of muscle activation distribution
7. Comparison of current methods and new methods

Bibliography / sources:

Hirashima, M. and Oya, T. (2016) 'How does the brain solve muscle redundancy? Filling the gap between optimization and muscle synergy hypotheses', Neuroscience Research, 104, pp. 80–87.
Mileusnic, M.P. et al. (2006) 'Mathematical Models of Proprioceptors. I. Control and Transduction in the Muscle Spindle', Journal of Neurophysiology, 96(4), pp. 1772–1788. Available at: <https://doi.org/10.1152/jn.00868.2005>.
Mileusnic, M.P. and Loeb, G.E. (2006) 'Mathematical Models of Proprioceptors. II. Structure and Function of the Golgi Tendon Organ', Journal of Neurophysiology, 96(4), pp. 1789–1802. Available at: <https://doi.org/10.1152/jn.00869.2005>.

Name and workplace of master's thesis supervisor:

prof. RNDr. Matej Daniel, Ph.D. České vysoké učení technické v Praze, Fakulta strojní

Name and workplace of second master's thesis supervisor or consultant:

Date of master's thesis assignment: **24.04.2023** Deadline for master's thesis submission: **13.08.2023**

Assignment valid until: _____


prof. RNDr. Matej Daniel, Ph.D.
Supervisor's signature

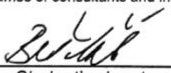

Head of department's signature


doc. Ing. Miroslav Španiel, CSc.
Dean's signature

III. Assignment receipt

The student acknowledges that the master's thesis is an individual work. The student must produce his thesis without the assistance of others, with the exception of provided consultations. Within the master's thesis, the author must state the names of consultants and include a list of references.

25.2023
Date of assignment receipt


Student's signature

Declaration

I hereby confirm that I conducted the research presented in this thesis entirely on my own. My supervisor provided guidance, and I consulted relevant literature. I used intelligence tools in grammar correction and code debugging while preparing this work. After using this tool, I reviewed and edited the content as needed, and I accepted full responsibility for the publication's content. All sources have been correctly cited, and this work is the result of my own efforts.

.....

Jiří Bešťák

In Prague, 2023

Acknowledgments

I would like to thank my thesis supervisor, prof. RNDr. Matej Daniel, Ph.D., for his willingness, valuable advice, professional guidance, and, most importantly, the time he devoted to me during the thesis preparation process. I would also like to thank my family and friends for their support.

Annotation list

Author name: Jiří Bešťák

Thesis name: Muscle activity driven by proprioception

Czech name: Řízení svalové aktivity pomocí propriocepce

Year: 2023

Study programme: (AVSI) Applied Science in Mechanical Engineering

Department: Department of Mechanics, Biomechanics and Mechatronics

Supervisor: prof. RNDr. Matej Daniel, Ph.D.

Bibliographic data: no. pages: 71
no figures: 51
no. tables: 9
no. attachments: 1

Keywords: Golgi tendon organ, proprioception, muscle activity, musculoskeletal model, optimization

Klíčová slova: Golgiho šlachové tělísko, propriocepce, svalová aktivita, svalově kosterní model, optimalizace

Annotation:

The exact mechanism how the brain generates muscle-proprioceptive patterns remains unknown. Currently, there exist several models of muscle movement control, but they centred on the issue of activation. The role of proprioception in the biomechanical assessment of muscle forces is mostly neglected. The aim of this thesis was to test the hypothesis that the muscle activation pattern can be obtained by a minimization of brain inputs from proprioceptors. We created a musculoskeletal model of elbow motion with 4 flexors and 3 extensors, integrated Golgi tendon-based proprioception with linear and nonlinear models. We have shown that the Hill-Langmuir nonlinear model approximates EMG measurements of elbow motion well. To conclude, we have defined a physiologically based criterium for muscle activations that can be verified in the further studies.

Anotace:

Přesný mechanismus, jakým mozek vytváří svalově-proprioceptivní vzorce, zůstává neznámý. V současné době existuje několik modelů řízení svalových pohybů, které se však soustředí na problematiku aktivace. Úloha propriocepce při biomechanickém hodnocení svalových sil je většinou opomíjena. Cílem této práce bylo ověřit hypotézu, že vzor aktivace svalu lze získat minimalizací mozkových vstupů z proprioceptorů. Vytvořili jsme muskuloskeletální model pohybu v lokti se 4 flexory a 3 extenzory, integrovali jsme propriocepci založenou na Golgiho šlachách s lineárními a nelineárními modely. Ukázali jsme, že Hill-Langmuirův nelineární model dobře aproximuje EMG měření pohybu v lokti. Na závěr jsme definovali fyziologicky podložená kritéria pro svalové aktivace, která lze ověřit v dalších studiích.

List of abbreviations

BRA	musculus brachialis
BICbre	musculus biceps brevis
BIClon	musculus biceps longus
BRD	musculus brachioradialis
CNS	central nervous system
COG	centre of gravity
DAS	dynamic arm simulator
GTO	Golgi tendon organs
MU	motor unit
MS	muscle spindle
PCSA	physiological cross-sectional area of muscle
TRIlon	musculus triceps longus
TRIlat	musculus triceps lateralis
TRImed	musculus triceps medialis
w.	with
w.o.	without
SLSQP	sequential least squares quadratic programming
2D	two-dimensional area

List of symbols

n	$[-]$	no. degree of motion
m	$[kg]$	weight of the segment
W_1	$[N]$	forearm force
W_2	$[N]$	hand force
r_{w1}	$[m]$	distance from elbow to COG of forearm
r_{w2}	$[m]$	distance from to COG of forearm to COG of hand
i	$[-]$	no. segments
r	$[-]$	no. revolute restraint
t	$[-]$	no. prismatic restraint
g	$[-]$	no. general restraint
ri	$[-]$	no. rigid restraint
c	$[-]$	no. cylindrical restraint

$\varphi(t)$	[deg]	time-dependent angle
φ_{max}	[deg]	maximum angle- full extension
φ_{min}	[deg]	minimum angle- full flexion
ω	[1/s]	angular velocity
φ_m	[deg]	medium angle value
φ_a	[deg]	maximum angle value
\vec{M}_{Mi}	[Nm]	torque vector generated by a muscle force
\vec{M}_V	[Nm]	torque vector generated by a force of gravity
\vec{r}_i	[m]	vector of moment arm
\vec{F}_i	[N]	vector of muscle force
\vec{e}	[—]	unit vector
f	[—]	scalar value of muscle force
\vec{r}_P	[m]	vector of proximal attachment
\vec{r}_D	[m]	vector of distal attachment
\bar{R}	[—]	matrix of rotation
y		individual computing parameter of segment
x_1	[kg]	weight of human body
x_2	[cm]	height of human body
b_i	[—]	coefficient for individual parameter of segment
F^M	[N]	total muscle force
F_0^M	[N]	maximal isometric force of the muscle
f_L^{active}	[—]	active force-length relation
f_v	[—]	force-velocity factor
a	[—]	activation
$f_L^{passive}$	[—]	passive force-length relation
α	[deg]	pennation angle
α_0	[deg]	pennation angle at optimal muscle length
σ_i	[N/cm ²]	stress of i -th muscle
L^M	[m]	actual muscle length
L_0^M	[m]	optimal muscle length
L^{MT}	[m]	total length of the musculotendon complex
L_S^T	[m]	tendon slack length

v_0^M	[m/s]	optimal velocity of muscle contraction
v^M	[m/s]	actual velocity of muscle contraction
a'	[N]	constant in Hill type muscle model
b'	[mm/s]	constant in Hill type muscle model
c	[−]	constant in Hill type muscle model
G_l	[−]	objective function, $l=1,...,12$
λ_i	[−]	weight of each muscle
t_0	[s]	the first time-step equal to 0
t_{end}	[s]	the last time-step equal to 2
N_{GTOi}	[−]	number of Golgi tendon organ
ρ_{MSi}	[1/g]	density of muscle
m_i	[g]	mass of muscle
F_{1i}	[N]	force from one muscle fascicle
A	[impluses/s]	constant in Lin and Crago nonlinear model
B	[N]	constant in Lin and Crago nonlinear model
r_i	[impluses/s]	response of single GTO
K	[−]	number of time steps in the variability model
k	[−]	Hill coefficient

List of figures

Figure 1: Structure of skeletal muscle [4]	16
Figure 2: Connection between muscle and CNS [6]	17
Figure 3: Simplified scheme of classification of motor nervous system	18
Figure 4: Scheme of the reflex circuit	18
Figure 5: Simplified scheme of the functioning of the spinal level of motor control	19
Figure 6: The patellar reflex - example of the stretch reflex [28]	19
Figure 7: Schematic drawing of the two main muscle proprioceptors [19]	20
Figure 8: The structure of GTOs [8]	21
Figure 9: Realistic GTO in mammals [11]	21
Figure 10: A - structure of MS [29] and B - realistic picture of MS [11]	22
Figure 11: Hill's muscle model [20]	23
Figure 12: The passive and active force – length relations [22]	24
Figure 13: The force-velocity relation A- when the activation level is $a(t)=1$ and B-when the activation level is $a(t)=0.5$ [20]	24
Figure 14: Scheme of forward dynamics [36]	26
Figure 15: Scheme of inverse dynamics (a) conventional two optimization loops for estimation of muscle forces and activation signals, (b) machine learning model for muscle force estimation and one optimization loop for activation signals, and (c) machine learning model for activation signals estimation [36]	26
Figure 16: A-scheme of the stretch reflex. B- GTO model [27]	28
Figure 17: Higher plots-muscle response to stretch and shortening. Lower plots- model afferent signals and the command to the extrafusal muscle [27]	29
Figure 18: A structure of the GTO model [8]	30
Figure 19: Response result of GTO model during tetanic stimulation of slow MUs [8]	31
Figure 20: (A) Self- and (B) cross-adaption result of the GTO model [8]	31
Figure 21: Nonlinear summation result of the GTO model [8]	32
Figure 22: Concept of proprioceptive prosthesis. Crosshatched part is developed by [25]	33
Figure 23: Scheme of the presented model. A - overall system model. B- static optimization model [25]	33
Figure 24: Predicted proprioceptor firing patterns during brushing the teeth. A - predicted primary afferent firing patterns and B - predicted GTO firing patterns [25].	34
Figure 25: Muscle activity of elbow flexors: (Left- m. brachialis, middle- m. biceps longus, right-m. biceps brevis) [44]	35

Figure 26: Muscle activity of selected muscles during elbow flexion (dark) and extension (light): (Left- m. triceps brachii, middle- m. biceps brachii, right-m. brachioradialis) [45]....	36
Figure 27: Average EMG for elbow flexor and extensor muscles of young subjects during the constant-load task. Left – 10% of 1-RM. Right-35 % of 1-RM [46].....	36
Figure 28:Project flowchart. Red-inputs, blue-computing, green-results.	38
Figure 29: The musculoskeletal model in OpenSim software with 7 muscles [39].....	39
Figure 30: Geometry of the upper arm. 1- frame, 2-upperarm, 3-forearm with hand, A- full flexion, B-full extension, C- general position.	40
Figure 31: Release of the forearm in general position	41
Figure 32: Rotating of coordinate system 2	41
Figure 33: Hill type muscle model [20]	44
Figure 34: Curves dependent on coefficient k. where k=1 is red curve, k=2 is orange curve, and k=4 is purple curve	49
Figure 35: Optimized loading in individual muscles with G_1 objective function. (Left - w.o. added weight in hand. Right-w. added weight in hand).	54
Figure 36: Optimized loading in individual muscles with G_2 objective function. (Left - w.o. added weight in hand. Right-w. added weight in hand).	54
Figure 37: Optimized loading in individual muscles with G_3 objective function. (Left - w.o. added weight in hand. Right-w. added weight in hand).	55
Figure 38: Optimized loading in individual muscles with G_4 objective function. (Left - w.o. added weight in hand. Right-w. added weight in hand).	55
Figure 39: Optimized loading in individual muscles with G_5 objective function. (Left - w.o. added weight in hand. Right-w. added weight in hand).	56
Figure 40: Optimized loading in individual muscles with G_6 objective function. (Left - w.o. added weight in hand. Right-w. added weight in hand).	56
Figure 41: Optimized loading in individual muscles with G_7 objective function. (Left - w.o. added weight in hand. Right-w. added weight in hand).	57
Figure 42: Optimized loading in individual muscles with G_8 objective function. (Left - w.o. added weight in hand. Right-w. added weight in hand).	57
Figure 43: Optimized loading in individual muscles with G_9 objective function. (Left - w.o. added weight in hand. Right-w. added weight in hand).	58
Figure 44: Optimized loading in individual muscles with G_{10} objective function. (Left - w.o. added weight in hand. Right-w. added weight in hand).	58

Figure 45: Optimized loading in individual muscles with G_{11} objective function, $k=4$. (Left - w.o. added weight in hand. Right-w. added weight in hand).	59
Figure 46: Optimized loading in individual muscles with G_{11} objective function, $k=2$. (Left - w.o. added weight in hand. Right-w. added weight in hand).	59
Figure 47: Optimized activations in individual muscles with G_2 objective function. (Left - w.o. added weight in hand. Right-w. added weight in hand).	61
Figure 48: Optimized activations in individual muscles with G_{10} objective function. (Left - w.o. added weight in hand. Right-w. added weight in hand).	61
Figure 49: Optimized activations in individual muscles with G_{11} objective function, $k=4$. (Left - w.o. added weight in hand. Right-w. added weight in hand).	62
Figure 50: Optimized activations in individual muscles with G_{11} objective function, $k=2$. (Left - w.o. added weight in hand. Right-w. added weight in hand).	62
Figure 51: Differences in the muscle force predictions between linear and nonlinear criteria [47].	65

List of tables

Table 1: Examples of some selected optimization criteria with constraints. F_i - muscle force of i -th muscle, σ_i - muscle stress of i -th muscle, w_i – coefficients [34]	27
Table 2: Coefficients for forearm and hand [37]	42
Table 3: Parameters of the forearm and the hand	42
Table 4: Parameters of Muscles.....	43
Table 5: Parameters of optimization.....	43
Table 6 Weight and density of MSs of i -th muscle	50
Table 7: Parameters of optimization.....	51
Table 8: Optimization criteria for GTO distribution	52
Table 9: Results of GTO optimization with using the Hill-Langmuir equation with the Hill type muscle model.....	60

Content

1	INTRODUCTION	15
2	STATE OF ART.....	16
2.1	MUSCLE	16
2.1.1	<i>Skeletal Muscle Structure and Function.....</i>	<i>16</i>
2.2	MUSCLES AND CONNECTION WITH CENTRAL NERVOUS SYSTEM	17
2.2.1	<i>Motor Control</i>	<i>17</i>
2.2.2	<i>Spinal Cord Level of Movement Control</i>	<i>18</i>
2.2.3	<i>Monosynaptic Stretch Reflex</i>	<i>19</i>
2.3	PROPRIOCEPTORS	20
2.3.1	<i>Golgi Tendon Organs</i>	<i>20</i>
2.3.2	<i>Muscle Spindle</i>	<i>22</i>
2.4	MATHEMATICAL MODELS OF MUSCLE	23
2.4.1	<i>Hill Type Muscle Model.....</i>	<i>23</i>
2.5	OPTIMIZATION METHODS FOR SOLVING BIOMECHANICS PROBLEMS.....	25
2.6	METHODS USED FOR MUSCLE ACTIVITY DRIVEN BY PROPRICEPTION	28
2.6.1	<i>Model of Proprioceptors I.</i>	<i>28</i>
2.6.2	<i>Model of Proprioceptors II.</i>	<i>30</i>
2.6.3	<i>Model of Proprioceptors III.</i>	<i>33</i>
2.7	EMG MEASUREMENTS OF MUSCLE ACTIVITY.....	35
3	AIM OF THE THESIS	37
4	METHODS	38
4.1	MUSCLE FORCE ASSESSMENT THROUGH INPUTS.....	39
4.1.1	<i>Musculoskeletal Model.....</i>	<i>39</i>
4.1.2	<i>Input Data.....</i>	<i>42</i>
4.1.3	<i>Optimization</i>	<i>43</i>
4.1.4	<i>Hill Type Muscle Model in Optimization</i>	<i>43</i>
4.2	MUSCLE FORCE ASSESSMENT THROUGH OUTPUTS	46
4.2.1	<i>Linear Model.....</i>	<i>46</i>
4.2.2	<i>Variability Model</i>	<i>47</i>
4.2.3	<i>Lin and Crago Model.....</i>	<i>47</i>
4.2.4	<i>Hill-Langmuir Model.....</i>	<i>48</i>
4.2.5	<i>Input Data and Optimization</i>	<i>50</i>
4.3	GOLGI TENDON ORGAN DISTRIBUTION	52
5	RESULTS	53

5.1	OPTIMIZED INPUTS	54
5.2	OPTIMIZED OUTPUTS	55
5.3	GOLGI TENDON ORGAN DISTRIBUTION	59
5.4	COURSE OF MUSCLE ACTIVATION IN SELECTED MODELS	61
6	DISCUSSION	63
7	CONCLUSION	66
8	SOURCES	67
9	APPENDIX	71
9.1	APPENDIX 1.....	71

1 Introduction

Neuromuscular models of proprioceptive control of muscle activity may, in the future, become an important part of biomechanics in the development of orthoses or prostheses. Slowly, more and more studies are progressing further and primary deal with the reverse problem: What is the process of information return to the brain? How does the brain know if a muscle is working properly or not? Nobody knows how the brain generates signals of muscle-proprioceptive patterns. The aim is to mimic these patterns to better understand how neuromuscular feedback works. An orthosis or prosthesis that could give feedback to the patient would allow a new level of living with disabilities.

2 State of Art

Muscle activity driven by proprioception is a broad topic including two large fields of study (physiology, biomechanics). For a better understanding of this issue, it is necessary to describe the basic terms of these areas.

2.1 Muscle

Muscle tissue is particularly specialized for motion, and it is one of the excitable tissues with the basic functional property of contraction and relaxation. There exist three main types of muscle tissue: smooth muscle, cardiac muscle, and skeletal muscle. For our purpose, we will further focus only skeletal muscle.

2.1.1 Skeletal Muscle Structure and Function

Skeletal muscles constitute to 45% of the body weight and form the motor component of the locomotion system. In general, muscle consists of origin, insertion, muscle belly, tendon and fascia. The fundamental structure unit is the muscle fibre, which consists of longitudinally oriented shrinkable myofibrils [2,3].

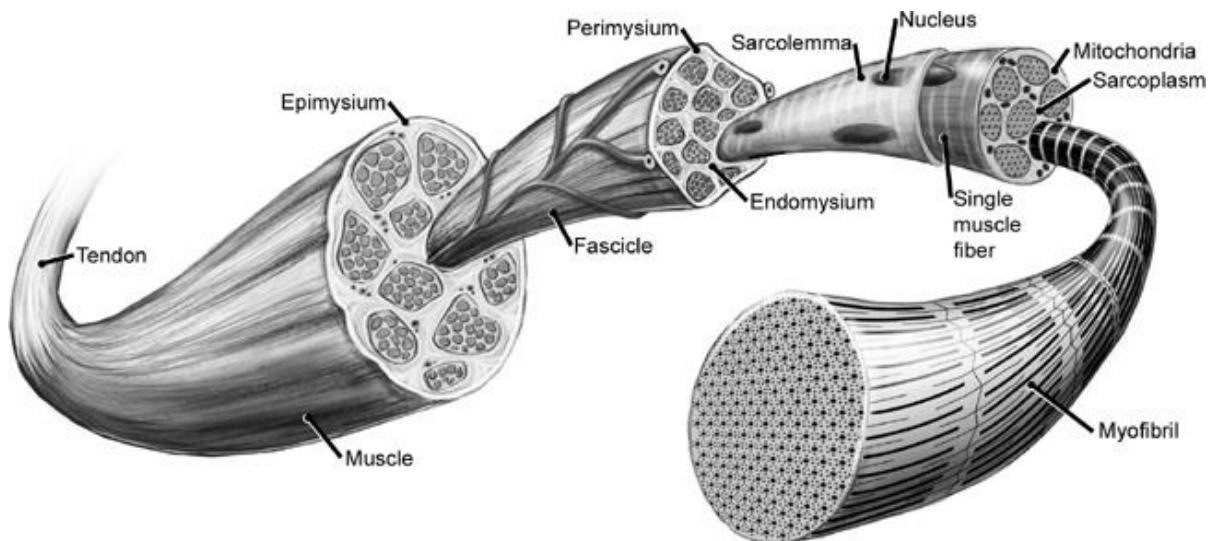


Figure 1: Structure of skeletal muscle [4]

The entire muscle is composed of bundles of muscle fibres, and it is encased in a layer of epimysium, which is part of fascia (Fig. 1). Bundles of muscle fibres are protected by a layer of perimysium and between each muscle fibres lies soft and thin layer of collagen fibres called endomysia. The surface of the muscle fibres forms cell membrane called the sarcolemma [1,2].

Muscles allow for overall posture of the body, motion of the whole body and its individual parts. Main function of muscle fibres is their stretch – contraction. The contraction is provided by myofibrils which consist of actin and myosin myofilaments. These small units are fixed between the Z lines. During contraction, this leads to stretching of the muscle, as thin actin and strong myosin myofilaments slide in between each other [2, 31].

2.2 Muscles and Connection with Central Nervous System

Most of the muscle fibres are innervated by only one motoneuron (motor nerve ending) through a neuromuscular disc. The presynaptic part of the neuromuscular disc is composed of axon terminals of a spinal motoneuron which can transmit action potential. This structure is a type of chemical synapse with its function being to transmit impulse from the neuron to the muscle fibres. A group of muscle fibres innervated by one motoneuron is called motor unit (MU) and it is also the smallest component which can be individually activated (Fig. 2) [1,2,3,5].

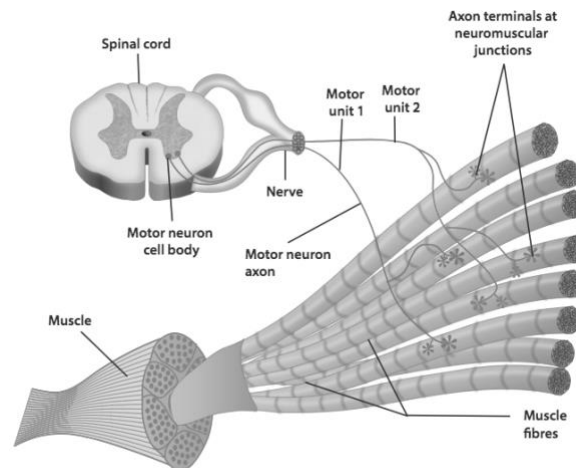


Figure 2: Connection between muscle and CNS [6]

According to the required muscle strength, the number of active MUs increases. This is called recruitment. At a low level of contraction, mainly slow tonic type of muscle fibres are recruited. The fast type of muscle fibres is recruited for the requirement of larger strength. In general, recruitment is organized from the activation of the smallest motoneurons to activation of the biggest motoneurons. This principle is used to reduce muscle and neuron fatigue [1,2].

2.2.1 Motor Control

Motor control or the motor nervous system is responsible for the control of muscle activity. The entire CNS is involved in motor control, and motor structures are hierarchically organized and interact with each other. Three basic levels are involved in movement control: spinal cord,

subcortical and cortical (Fig. 3). In our thesis, the most important level of movement control is spinal level. Realistic control of movement is much more complicated [1,5].

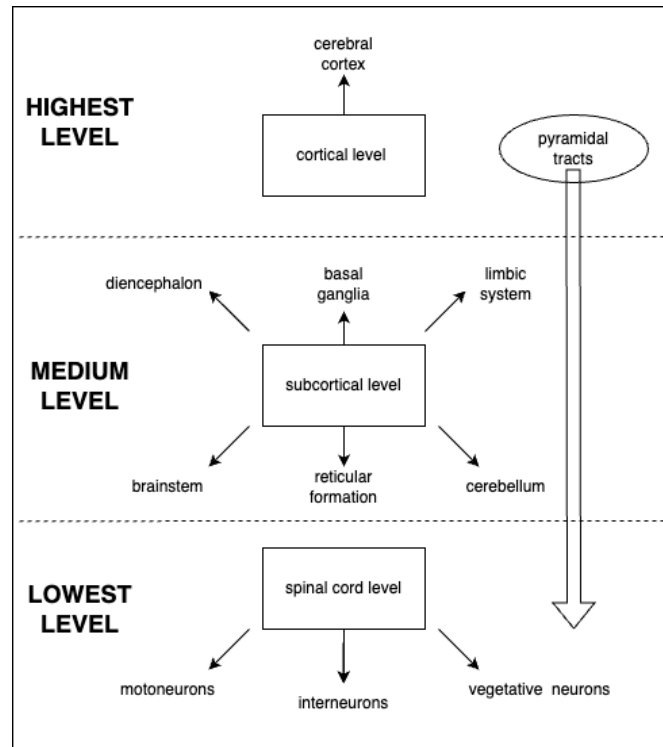


Figure 3: Simplified scheme of classification of motor nervous system

2.2.2 Spinal Cord Level of Movement Control

Primary segment of movement control is spinal cord, which is also subordinate to the higher divisions of the nervous system. The main role is played by motoneurons, interneurons, and vegetative neurons. Each neuron has the function of transmitting excitation. This transmission and control are based on the reflex principle (Fig. 4) [1,5].

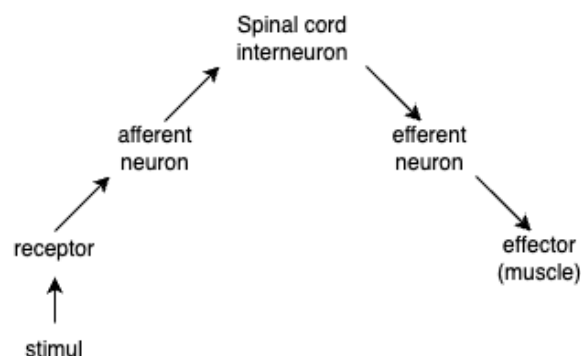


Figure 4: Scheme of the reflex circuit

The motoneurons include α -motoneurons and γ -motoneurons. α -motoneurons are located in the anterior corners of the spinal cord, and they end at the neuromuscular disc. Their function

is communication between muscle and the nervous system. γ -motoneurons refine movements, affect inter-muscular coordination, and communicate with muscle bundles. Interneurons have both excitatory and inhibitory function, allowing them to communicate with subcortical and cortical levels of movement control. They are located in the grey matter of spinal cord. Vegetative neurons provide control logistics. The spinal level of movement control works as shown in Fig. 5 below [1,5].

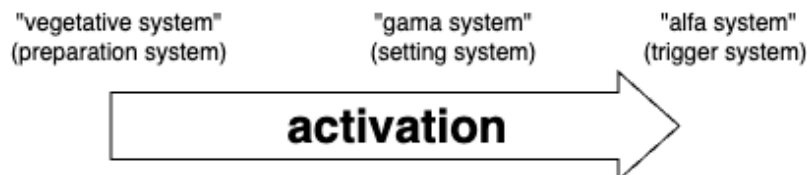


Figure 5: Simplified scheme of the functioning of the spinal level of motor control

2.2.3 Monosynaptic Stretch Reflex

The stretch reflex is one of the examples of a monosynaptic and spinal reflex. It is a very fast response of the muscle to its stretching and has the shortest latency of all spinal reflexes. This reflex is initiated when the muscle spindle (MS) detects stretch or lengthening of the muscle. Then, the MS sends a signal to the spinal cord through afferents nerve fibres (Fig. 6). These afferents nerve fibres end at α -motoneurons in the anterior corners of the spinal cord. Then the spinal cord generates an immediate reflexive response. It sends signals to activate the motor neurons, causing the stretched muscle to contract. Simultaneously, the spinal cord also inhibits the motoneurons of the antagonistic muscle. This coordinated contraction and relaxation response helps to act the stretching force and keep muscle tone. Examples of the stretch reflex are the patellar reflex, biceps reflex, triceps reflex, jaw jerk reflex or Achilles reflex [1].

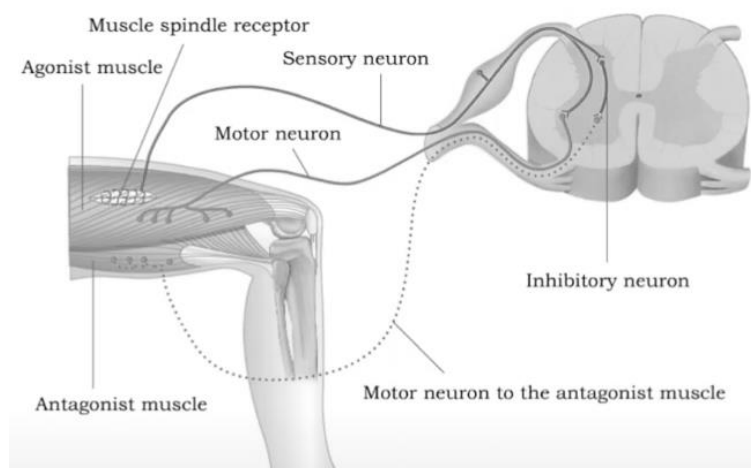


Figure 6: The patellar reflex - example of the stretch reflex [28]

2.3 Proprioceptors

The word proprioceptor comes from the Latin proprius – meaning “own” and capio – meaning “accept” or “to take”. The term of proprioception dates back to the late 19th and early 20th centuries. Proprioception is sensory system that allows us to perceive afferent information about the position of our muscles, tendons, joints and other tissues in our body. It is, therefore, a part of the nerve system with the ability to perceive changes and give us proprioceptive feedback to control our bodies. This capability makes possible the use of sense receptors – mechanoreceptors which are mechanosensory neurons. Signals are transmitted through these mechanosensory neurons to the central nervous system, where they combine further information from other sensory systems (Fig. 7). This process thus creates an overall model of the location, movement and acceleration of the body [1,21].

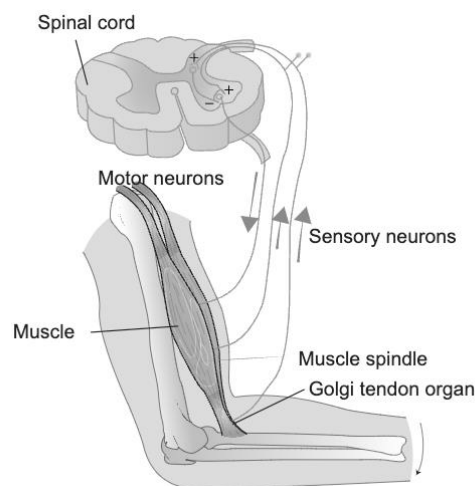


Figure 7: Schematic drawing of the two main muscle proprioceptors [19]

Proprioceptors include joint receptors, receptors of ligament tissue, GTOs and MSs. Of these, the last two are the most important for our thesis. All of them share one common feature – they probably cannot regenerate, and their number decreases with age and diseases [7].

2.3.1 Golgi Tendon Organs

GTOs are tension-sensitive mechanoreceptors situated at the musculotendinous junction, and which is the interface between muscle and tendon. They provide the CNS information about muscle tension through their Ib afferent nerve fibre. Mostly, their distribution is uneven, and they lie deep in the muscle core [8].

In rare cases, they can be located within the tendon themselves [9], and also, we can find cases [7] in which some Ruffini corpuscles (another type of mechanoreceptors) resemble GTOs. The number of GTOs is smaller than the number of muscle spindles and ranges between 10-100

[10]. GTOs are placed in series between muscle and tendon, and they consist of bundles of collagen fibre that connect small fascicles of muscle to the tendon or aponeurosis. Jami (1992) [10] claims that 5% of GTOs are attached to more than 25 muscle fibre.

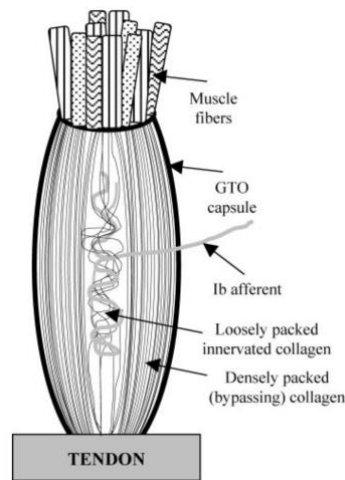


Figure 8: The structure of GTOs [8]

In the near of GTO's middle, the Ib afferent enters and travels to the center of GTO capsule, and then it divides into two or more branches (Fig. 8, Fig. 9). These branches are subsequently divided further into smaller branches until giving rise to unmyelinated collateral branches that intertwine among the strands of innervated collagen. GTOs contain of two types of collagen-the first one is innervated and lies in the GTO's capsule lumen, while the second one is located at the edge with densely packed and parallel oriented fibres [12,13].

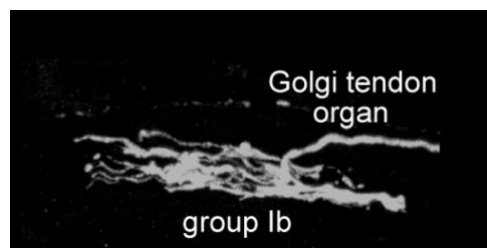


Figure 9: Realistic GTO in mammals [11]

If the MU is activated with at least one muscle fibre inserting into the GTOs, then some of the loosely placed collagen fibres are stretched, which will result in compressing and depolarizing the pressure-sensitive afferent ending, leading to the initiation of action potentials in the Ib afferent nerve fibre [14].

The GTOs have several interesting functions. Firstly, after a sudden step activation of the MU, the response of GTOs shows a quick increase in activity and then it gradually decreases to constant a afferent load. Secondly, the GTO response depends not only on tension but also on

the type of activated MU. This means that the same size of discharge frequency during activation can be triggered with both MUs with small force and great force. Thirdly, the observed phenomenon is that the GTO's dynamic response during the activation of the MU is decreased after the previous activation of the same or different MU. This is called self-adaption and cross-adaption. When the MUs are stimulated in the GTO at the same time, the GTO response is lower than the sum of GTO response during stimulation, which individual MU produces independently [15,16,17,18].

2.3.2 Muscle Spindle

MSs are also sensitive mechanoreceptors found in mammal skeletal muscle. They are situated in parallel with extrafusal muscle fibres and they register stretching and shortening of the muscle. MSs have a crucial role in kinaesthesia and in reflexive adjustments to perturbations [29].

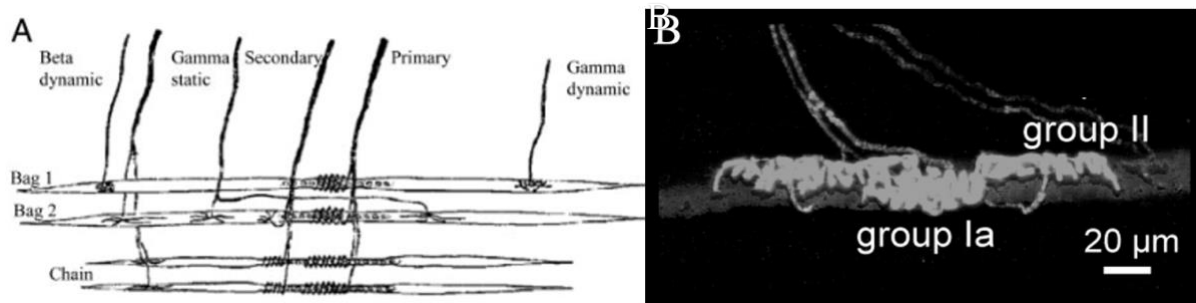


Figure 10: A - structure of MS [29] and B - realistic picture of MS [11]

Their afferents nerve fibres send information to the CNS about the length and velocity of the muscle. On the other hand, MS receives information from their static and dynamic specialized fusimotor efferents. As you can see in Fig 10A, the MS consists of three types of intrafusal muscle fibres – long nuclear fibres bag 1 and bag 2 and shorter chain fibres. Bag 1 is velocity-sense fibre and has dynamic fusimotor efferent endings. Bag 2 is a length-sense fibre and has static fusimotor efferent endings. All three types of intrafusal fibres are located near the equatorial zone of the MS, where they serve as primary afferents ending responsible for providing information about the length and velocity of the muscle [29].

2.4 Mathematical Models of Muscle

There are various mathematical models of muscles available at present. One option can be the Hodgkin-Huxley model, which considers both the mechanical and metabolic aspects of muscle contraction. Other muscle models, such as Zajac's, Thelen's, Millard's, can be also used. However, for our thesis, the widely used Hill type muscle model is important.

2.4.1 Hill Type Muscle Model

This three-element model is a representation of the muscle mechanical response. It is very popular for use in forward and inverse dynamics in optimization methods. The model consists of a muscle and tendon, which are presented as idealized mechanics objects. In this case, the muscle consists of an active force generator and a parallel passive component (Fig. 11) [20].

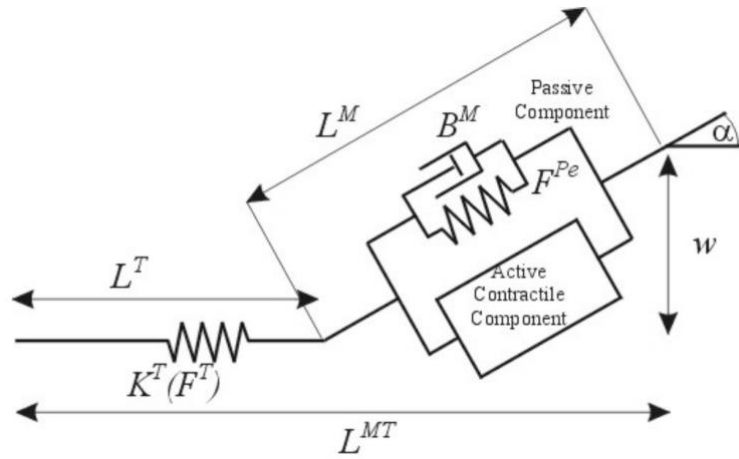


Figure 11: Hill's muscle model [20]

In this model, the total force of the complex is the sum of the passive and active forces, expressed by equation (1) [20]:

$$F^M = F_0^M (f_L^{active} f_v a(t) + f_L^{passive}) \cos(\alpha) \quad (1)$$

where is

F^M	total muscle force
F_0^M	maximal isometric force of the muscle
f_L^{active}	active force-length relation
f_v	force-velocity factor
a	activation
$f_L^{passive}$	passive force-length relation
α	pennation angle

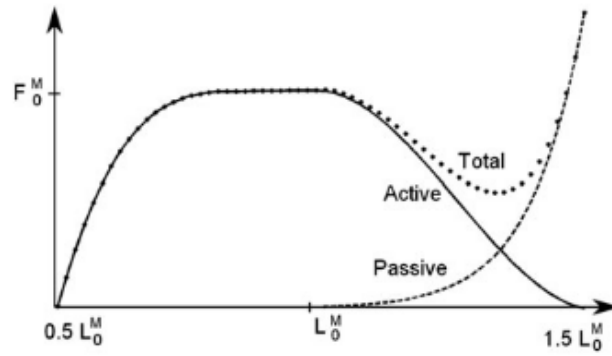


Figure 12: The passive and active force – length relations [22]

When the muscle is completely tetanized, the active force takes the shape of parabola, which is dependent on fibre length L^M in a nominal region $\langle 0.5 L^M_0, 1.5 L^M_0 \rangle$, with maximum force when $L^M = L^M_0$ (Fig. 12). Here is L^M actual muscle fibre length and L^M_0 is the optimal muscle fibre length. The passive force-length is an exponential function that describes muscle strengthening when the muscle is lengthened more than optimum muscle length. The dependence of muscle force and velocity contraction is different for eccentric and concentric contractions (Fig. 13) [20].

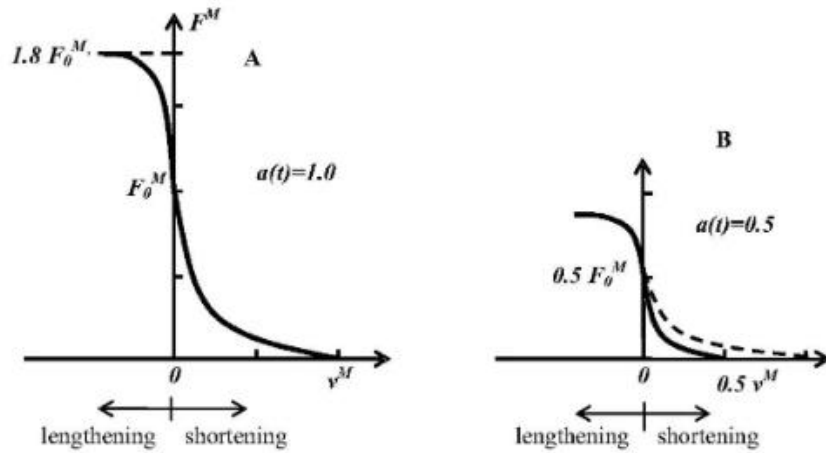


Figure 13: The force-velocity relation A- when the activation level is $a(t)=1$ and B-when the activation level is $a(t)=0.5$ [20]

2.5 Optimization Methods for Solving Biomechanics Problems

The musculoskeletal system of the human body, or its segments, is typically represented in mathematical models as a system of absolutely stiff segments interconnected by joints. The motion of the segments is the result of muscles spanning the joints. Thus, we can describe the human body as a multibody mechanical system directed by the equations of dynamic equilibrium. In general, simulating of the musculoskeletal system can be achieved through forward and inverse dynamics [34].

In cases where there are more muscles available than movements to produce, it is referred to as muscle redundancy. In other words, there are more muscles available than number of the associated equations of motion. Then the problem becomes mathematically indeterminate. This can be solved by methods that reduce the degree of muscle redundancy in the model or through methods that optimize the solution. Optimization methods aim to find the best combination of control based on a specific criterion. It is based on the cost or criterion function, which can be expressed as, for example: the resulting movement of the musculoskeletal model in response to a given control strategy. Currently, there is no optimization method with criteria that is directly used by our CNS. Biomechanics process like running or walking can be solved quasistatically, where each time step is considered independent of other time steps. Alternatively, they can be solved dynamically, where control decisions are made based on their impact on future steps. This dynamic optimization occurs over entire time interval necessary to accomplish the task. Quasistatic analyses are simpler, but dynamic analyses are more accurate. An example of a quasistatic approach is linear programming [34, 35].

For discovering the interact between the elements of the neuromusculoskeletal system during the production of movement, a dynamic solution is powerful approach. Forward dynamics provide the opportunity to change muscle excitation patterns or other parameters of the musculoskeletal model to understand how they affect movement. This type of the dynamic simulation analysis has been used, for example, in study of neural control of movement by Zajac (1993), in the design of neuromuscular stimulation systems by Yamaguchi and Zajac (1990), in evaluating the causes of pathological movement by Riley and Kerrigan (1998), and in design prosthetic devices by Piazza and Delp (2001). An example of a forward simulation of a musculoskeletal system is shown in Fig. 14 [33].

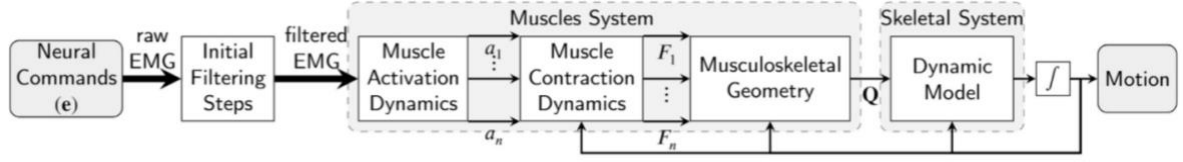


Figure 14: Scheme of forward dynamics [36]

In biomechanics, the inverse dynamics is often used to explore features of the control of movement, mechanics, and energetics. This approach is based on measuring the kinematics of the body segments, and it can also be based on measuring the external forces. Thus, the motion of the segments and external forces acting on the body are known. With this provided data, the joint reaction forces and joint torque are computed using Newton's equations of motion [32]. An example of an inverse simulation of a musculoskeletal system is shown in Fig. 15.

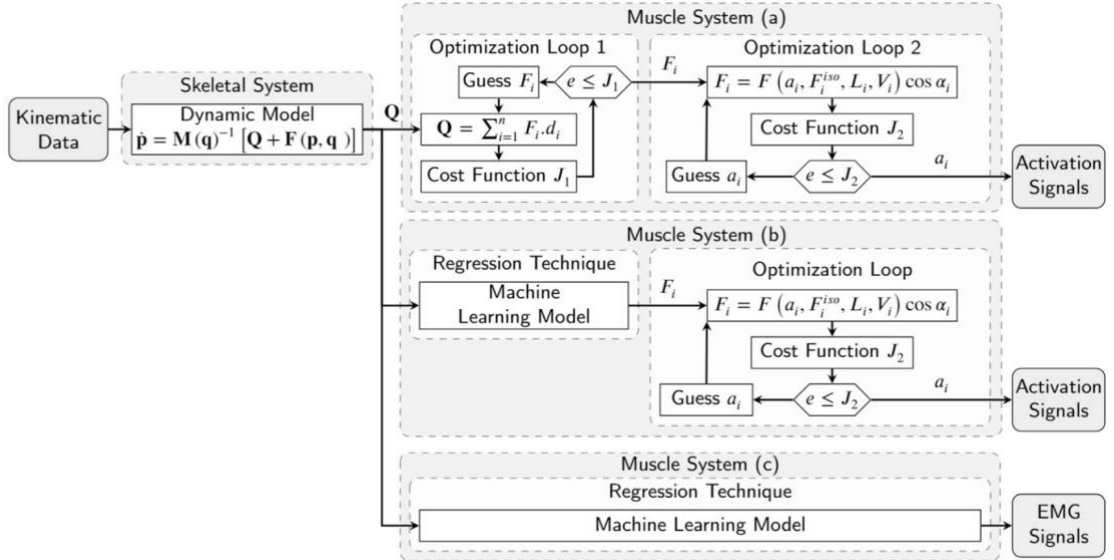


Figure 15: Scheme of inverse dynamics (a) conventional two optimization loops for estimation of muscle forces and activation signals, (b) machine learning model for muscle force estimation and one optimization loop for activation signals, and (c) machine learning model for activation signals estimation [36]

So far, several optimization criteria with constraints have been used by the scientific community at large. For example, in Tab. 1 is shown some criteria that are used for flexion in the elbow or for movement in the upper limb in general. These criteria are not the only ones, and many others can be used.

$\min \sum_i^n F_i^2 w_i$	$F_i \geq 0$
$\min \sum_i^n \sigma_i^2$	$\sigma_i \geq 0 \wedge \sigma_i \leq \sigma_{max}$
$\min \sum_i^n \sigma_i^3$	$\sigma_i \geq 0 \wedge \sigma_i \leq \sigma_{max}$
$\min \sum_i^n \sigma_i^{10}$	$\sigma_i \geq 0 \wedge \sigma_i \leq \sigma_{max}$
$\min \sigma_{max}$	$\sigma_i \geq 0$
$\max \sum_i^n \sqrt{1 - (\frac{F_i}{F_{max}})^2}$	$F_i \geq 0$

Table 1: Examples of some selected optimization criteria with constraints. F_i - muscle force of i -th muscle, σ_i - muscle stress of i -th muscle, w_i - coefficients [34]

2.6 Methods Used for Muscle Activity Driven by Proprioception

2.6.1 Model of Proprioceptors I.

Lin and Crago (2002) [27] developed a model for the stretch reflex of the musculus soleus in the decerebrate cat in MATLAB Simulink software. They combine a muscle model with the spindle model and develop models of GTO and the reflex pathways to complete a model of the stretch reflex. The input for this model is the force produced by the extrafusal muscle. This force is determined by the muscle activation level and the muscle length as well as the velocity. The output is an efferent command.

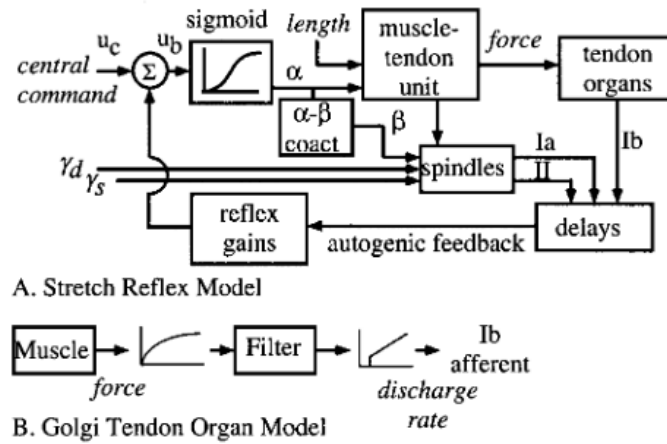


Figure 16: A-scheme of the stretch reflex. B- GTO model [27]

The muscle-tendon unit represents the extrafusal muscle (Fig. 16). MSs monitor muscle length, and GTOs monitor muscle force. The feedback signal from these proprioceptors interacts with the central command in the α -motoneuron pool with three components (reflex gains, a summer and a sigmoidal nonlinearity). The output of the motoneuron pool activates the extrafusal muscle and simultaneously activates intrafusal muscle fibres through the β efferents. Lin and Crago (2002) [27] used Hill type muscle model which is modified to demonstrate the yielding phenomenon by assuming that dynamics of activation and attachment are influenced by both the neural input and the length and velocity of the contractile element. For the MS, they used their own model.

The GTO model (Fig. 16B) is a force sensor with three components in series: a saturation nonlinearity, a phase lead filter, and a threshold nonlinearity [27]. Their model is based on the Houk's and Simon's model and assumes that the outputs of all GTOs are averaged to produce equal single feedback.

The responses of a muscle with and without reflex are different (Fig. 17). When a muscle with reflexes is stretched, the force constantly increases throughout the entire stretching period. When a muscle without reflexes is stretched, the force increases at a high slope in first place, and then the slope quickly decreases while the muscle is still stretched [27].

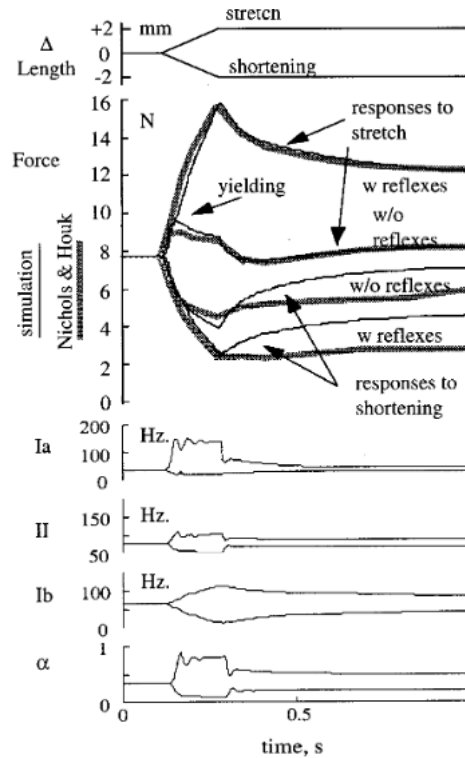


Figure 17: Higher plots-muscle response to stretch and shortening. Lower plots- model afferent signals and the command to the extrafusal muscle [27]

The type II afferent has higher sensitivity to static stimuli but lower sensitivity to dynamic stimuli compared to the Ia afferent. The overall reflex responses for both shortening and lengthening through ramp and hold are relatively symmetrical. On the other hand, the internal mechanical responses and the reflex contributions exhibit asymmetry [27].

2.6.2 Model of Proprioceptors II.

Mileusnic (2006) developed a mathematical model of GTO in MATLAB Simulink, which has the anatomical features of the biological receptor. This physiologically realistic model describes and contains [8]:

- The GTO's static and dynamic response
- The phenomena of GTO's self- and cross-adaptation
- Various degrees of nonlinear summation of GTO
- The relationship between the cross-adaptation and summation

The input for this model is tension from multiple muscle fibres inserted into its capsule. The model takes in tensions from 20 fibres that come from 13 different MUs. Each MU can have one or two fibres inserted to the receptor's capsule. The output of this model is GTO afferent activity. The complete GTO model has 64 nonlinear collagen springs and two dampers [8].

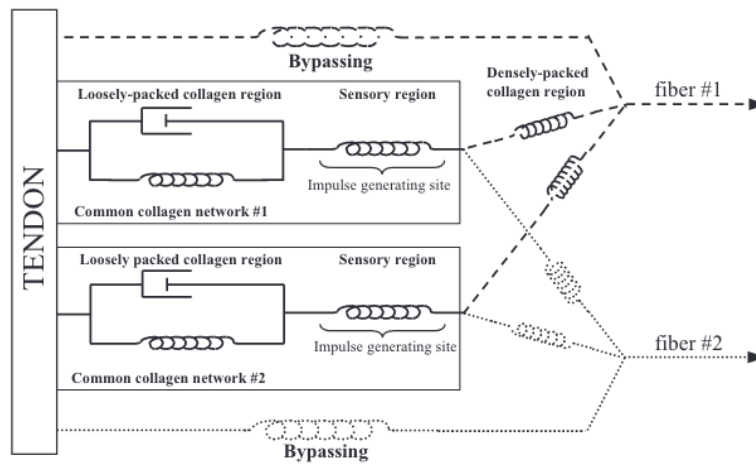


Figure 18: A structure of the GTO model [8]

For better visualization of the model structure, the figure represents only two muscle fibres inserted into the GTO capsule (Fig 18). Each fibre has its own collagen distributed among both innervated and bypassing collagen. These collagens are further divided among two distinct collagen networks. Each network has its own sites for generating impulses. The bypassing collagen refers to densely packed collagen that is connected to the muscle fibre inserted into the receptor but is not intertwined with the afferent endings. The innervated collagen is densely packed towards the ends of the capsule, but in the middle of the capsule, it becomes loosely arranged and intermingled with the afferent endings. All other features of the model structure correspond to various anatomical or physiological aspects, and they also correspond to the experimental literature [8].

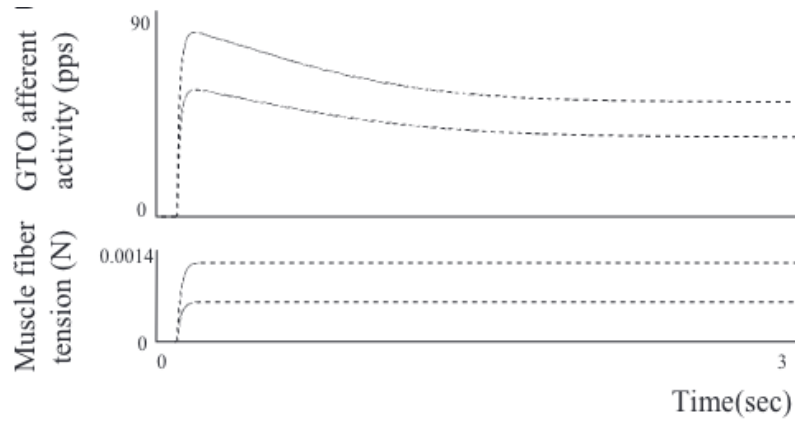


Figure 19: Response result of GTO model during tetanic stimulation of slow MUs [8]

The result of the GTO model response is shown in Fig. 19. This is the response during tetanic stimulation of slow MUs, which had either one or two of their fibres inserted into the GTO. The assumption is that innervated collagen is evenly distributed between the two common collagen networks [8].

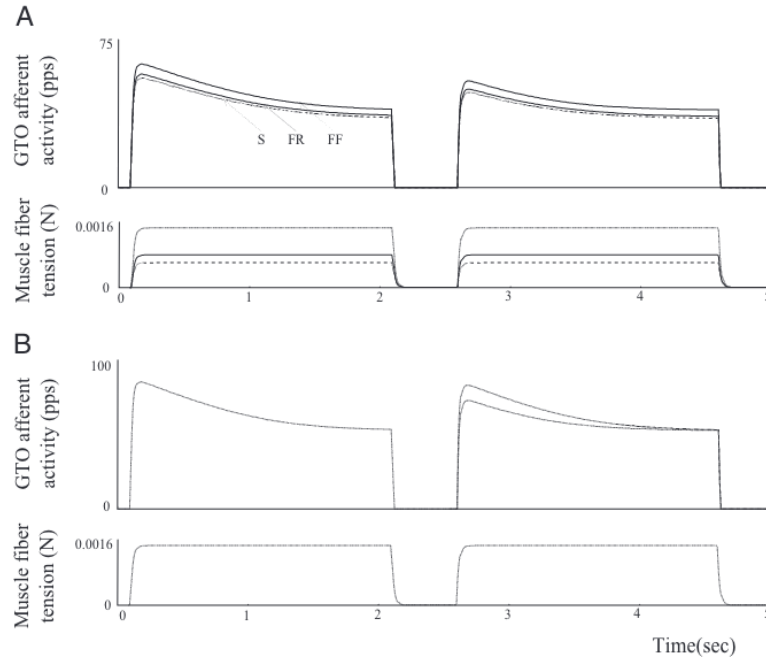


Figure 20: (A) Self- and (B) cross-adaption result of the GTO model [8]

Fig. 20 (A) demonstrates the self-adaptation of the GTO model. At first, [8] set the GTO model to the tetanic MU activation for 2 s (Fig. 20). Then the activation was removed and restored to the same MU after 0.5s. To demonstrate cross-adaption, the same pattern of activation was used as in self-adaption but with each burst of activation directed to a different muscle fibre.

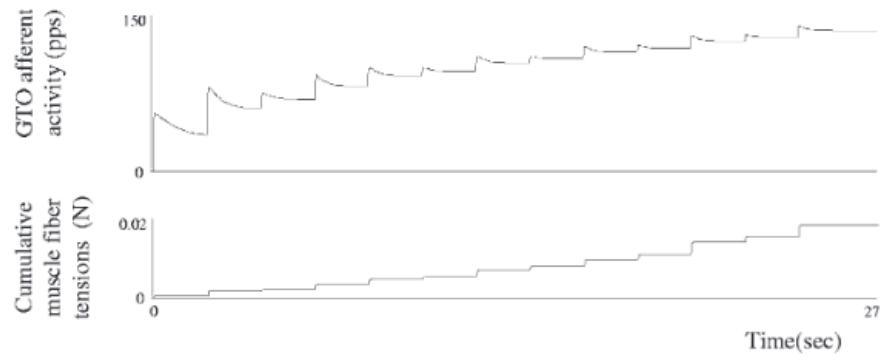


Figure 21: Nonlinear summation result of the GTO model [8]

Fig. 21 demonstrates the nonlinear summation of the GTO model. In this model, 13 MUs were activated one after the other in the order of natural recruitment – the first activated MUs are S (slow-twitch), then FR (fast-twitch oxidative-glycolytic), and then FF (fast-twitch glycolytic).

2.6.3 Model of Proprioceptors III.

Williams and Constandinou (2014) [25] developed a real-time model of proprioceptive signals from specific receptors. Their goal is to demonstrate the feasibility of the model and support future investigations into the potential benefits of imitating natural signal. They presented proprioceptive prosthesis processing concept for a transhumeral amputee, which includes mapping the movement of a prosthetic onto a human arm model for equivalent computing muscle, tendon, and receptor modulation (Fig. 22).

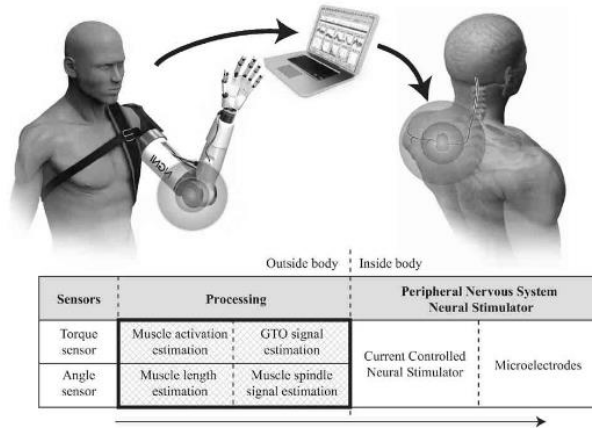


Figure 22: Concept of proprioceptive prosthesis. Crosshatched part is developed by [25]

The processing concept is about converting data from prosthesis sensors into estimations of proprioceptive neural signals from MSs and GTOs [25]. Their model concept is shown in Fig. 23.

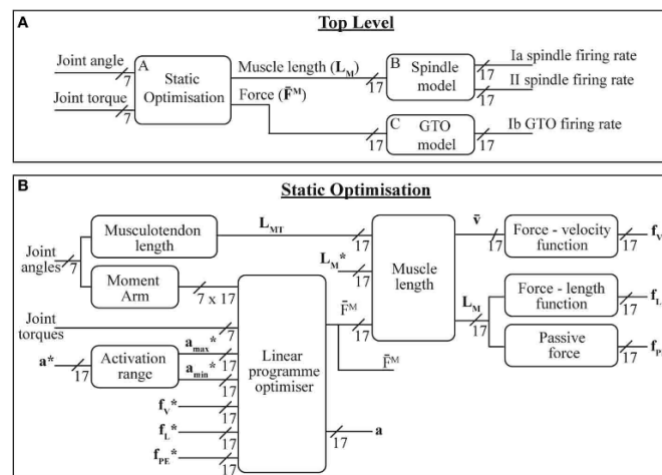


Figure 23: Scheme of the presented model. A - overall system model. B- static optimization model [25]

The input consists of joint angles and torques derived from the movements of an actor who swings his arms while walking across a room, then brushes his teeth before walking, and finally returns to the original position (Fig 23). This data was inserted into the musculoskeletal model

of the upper limb (Stanford VA Upper Limb) in OpenSim. They modified this model, which consists of 17 muscles, 7 degrees, thorax, sternum, scapula, clavicle, humerus, radius, ulna, wrist bones and 2nd to 5th metacarpals. They used Hill type muscle model, MS model proposed by [26], and GTO proposed by [27].

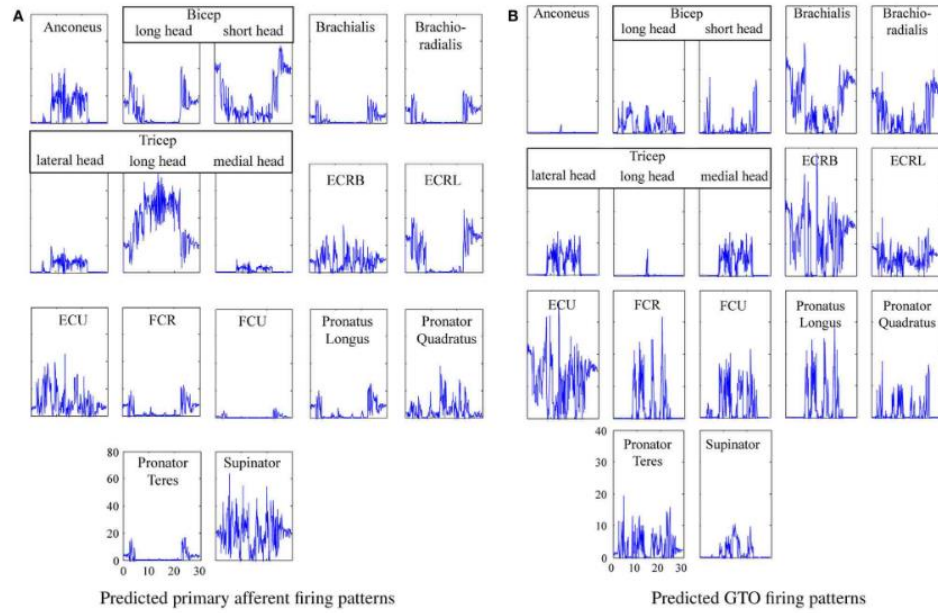


Figure 24: Predicted proprioceptor firing patterns during brushing the teeth. A - predicted primary afferent firing patterns and B - predicted GTO firing patterns [25].

The complete system output is presented in Fig.24. The system was executed to produce neural signals from primary afferents and GTO neural signals.

2.7 EMG Measurements of Muscle Activity

Electromyography (EMG) is an experimental method that serves for recording and analyzing myoelectric signals. It records intramuscular or surface muscle activity as well as the activity of the nerve that controls a particular muscle. This activity is registered and measured by an electromyograph which senses the action potential. The action potential is a signal that arises from peripheral nerve stimulation or muscle activation. This signal travels through the nerve fibres and leads to the activation of the muscle fibres that results of causing twitches or contractions. The electrodes record individual muscle contractions and transmit the data to a computer as an EMG waveform. The commonly used method for muscle activity assessment is amplitude analysis [43].

Date et al. (2021) [44] measured muscle activity of the elbow flexors with both surface and intramuscular EMG. They had a sample of six healthy men who were performing maximum isometric voluntary contractions and an isotonic elbow-flexion task without lifting any weight. In Fig. 25 is shown muscle activity of the elbow flexors (*m. brachialis*, *m. biceps longus* and *m. biceps brevis*) and comparisons between the surface and intramuscular during elbow-flexion task.

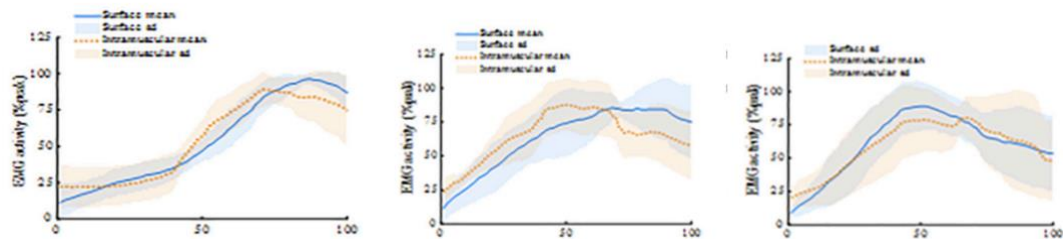


Figure 25: Muscle activity of elbow flexors: (Left- *m. brachialis*, middle- *m. biceps longus*, right-*m. biceps brevis*) [44]

Chaytor et al. (2020) [45] characterized the muscle activity of the arm during cycling at different relative workloads with 11 participants. In Fig. 26 is shown muscle activity of *m. triceps brachii*, *m. biceps brachii* and *m. brachioradialis*.

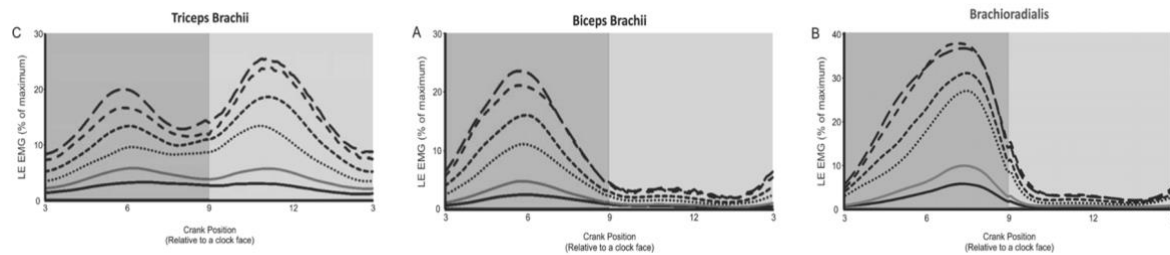


Figure 26: Muscle activity of selected muscles during elbow flexion (dark) and extension (light): (Left- *m. triceps brachii*, middle- *m. biceps brachii*, right-*m. brachioradialis*) [45]

Graves et al. (2000) [46] measured the activity of the elbow flexor muscles during both an isometric and an isotonic task. For this study, a total of 17 young subjects were recruited, who were seated in a modified chair, and their left arms were constrained to perform either isometric contractions or to lift inertial loads. Additionally, straps were placed over their shoulders to restrain the subjects and minimize shoulder motions. They defined the 1-RM load as the maximum amount of weight that could be lifted no more than once without using extraneous body movements. The 1-RM load was determined with the subject seated in the experimental chair. For this group of subjects, the average value of the 1-RM load was 17.5 ± 1.8 kg. In Fig. 27, we can observe the EMG measurement of muscle activity during elbow motion with 10% of 1-RM (1.75 kg) and with 35% of 1-RM (5.25 kg).

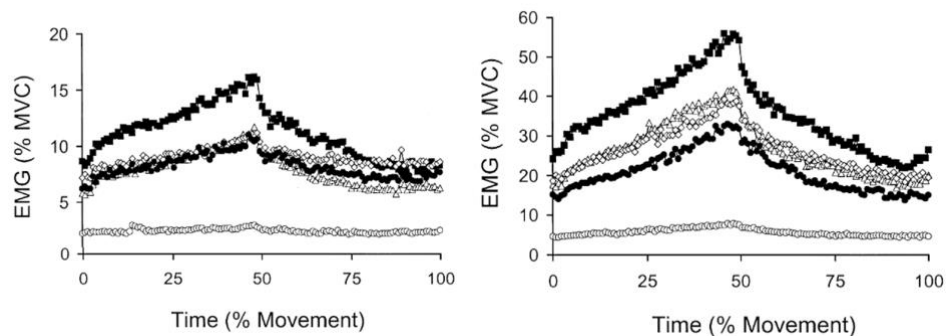


Figure 27: Average EMG for elbow flexor and extensor muscles of young subjects during the constant-load task. Left – 10% of 1-RM. Right-35 % of 1-RM [46].

3 Aim of the Thesis

Neuromuscular models of proprioceptive control of muscle activity may, in the future, become an important part of biomechanics in the development of orthoses or prostheses. Currently, there exist several models of muscle movement control, but they mainly focus on the issue of activation. Activation is followed by proprioception, which is mostly ignored. Based on these aims, we have chosen to define the following hypothesis:

“The optimal load for each muscle could be obtained by minimizing brain inputs from proprioceptors.”

We want to estimate forces generated from each muscle with the inclusion of proprioception. The specific aims of the thesis are:

- Develop a musculoskeletal model of the selected joint. We chose the elbow joint, specifically elbow motion (flexion and extension) in 2D.
- Demonstrate the solution of muscle redundancy through optimization methods.
- Develop and implement proprioception model of Golgi tendon organs (GTOs) into the musculoskeletal model.
- Present optimization criteria for this implementation.
- Comparison with current methods

For this issue, we aim to select a simple motion of a human joint that can be well verified either experimentally or through other studies. That is why we have chosen the elbow motion. We also chose to primarily work with freely available software such as Python or OpenSim. For this reason, we have developed a musculoskeletal model in Python. To implement optimizing methods, we selected the widely used *scipy.optimize* library with the SLSQP method in the Python software, which is suitable for solving inverse quasistatic problems in biomechanics.

4 Methods

The aim of this chapter is to present the methodology of the calculations that are the subject of this thesis. Firstly, the approach to solving muscle redundancy will be presented, and the basis of which is the solution to the muscle reduction through optimization methods. The anatomical musculoskeletal model of elbow motion and its solving muscle redundancy is described in the chapter 4.1. This model will be used to compare outputs as a result of the first part. In the chapter 4.2. is presented developing and implementation of proprioception model into the anatomical musculoskeletal model. Furthermore, additional models are presented for comparison of the outputs as a result of the second part. The third part is dual optimization problem of proprioception implementation where we try to set such a number of GTOs that will give us minimum output signal. The problems we consider in both parts of this chapter are solved quasistatically in the Python software. All optimization methods are calculated using the *scipy.optimize.minimize* with SLSQP method. Further details regarding each computing part are provided below. The overview of the thesis is shown in Fig. 28.

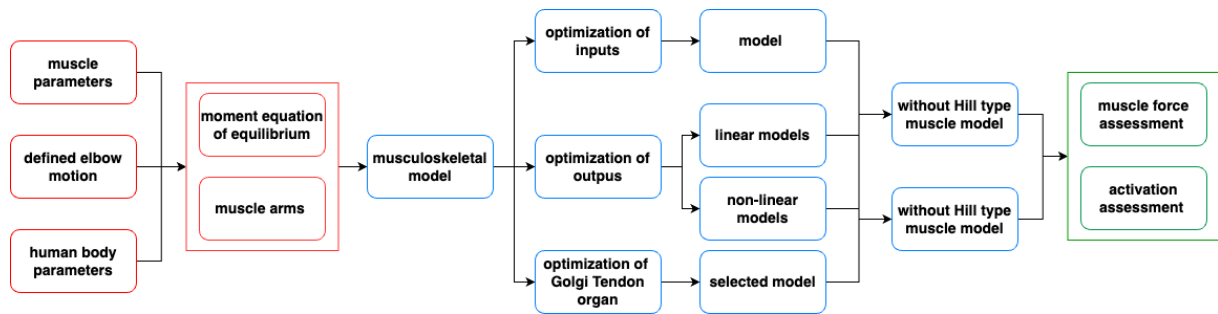


Figure 28: Project flowchart. Red-inputs, blue-computing, green-results.

4.1 Muscle Force Assessment through Inputs

In order to address muscle redundancy, it is necessary to create several fundamental computations. The goal is to establish and use a musculoskeletal model to obtain optimized forces from each muscle that participates during this motion.

4.1.1 Musculoskeletal Model

We assume the upper arm with a fixed shoulder joint, a free elbow, and a forearm in 2D. The forearm is rigidly connected to the wrist, resulting in a single segment. The upper arm is fixed in a position along the body. In this case, we also consider that the muscle is an ideal force generator. The motion is ensured by 7 muscles-4 flexors and 3 extensors (Fig. 29):

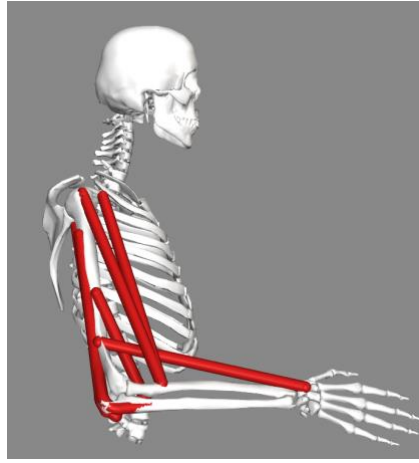


Figure 29: The musculoskeletal model in OpenSim software with 7 muscles [39]

- m. brachioradialis, m. brachialis, m. biceps c. brevis, m. biceps c. longus
- m. triceps lateralis, m. triceps longus, m. triceps medialis

In terms of mechanics, it is an open kinematic chain with one degree of freedom.

$$n = 3(i - 1) - 2r - 2t - 1g - 3ri - 2c \quad (2)$$

where is

i	no. segments
r	no. revolute restraint
t	no. prismatic restraint
g	no. general restraint
ri	no. rigid restraint
c	no. cylindrical restraint

$$n = 3(3 - 1) - 2r - 3f = 6 - 5 = 1^\circ \quad (3)$$

The geometry is shown in Fig. 30:

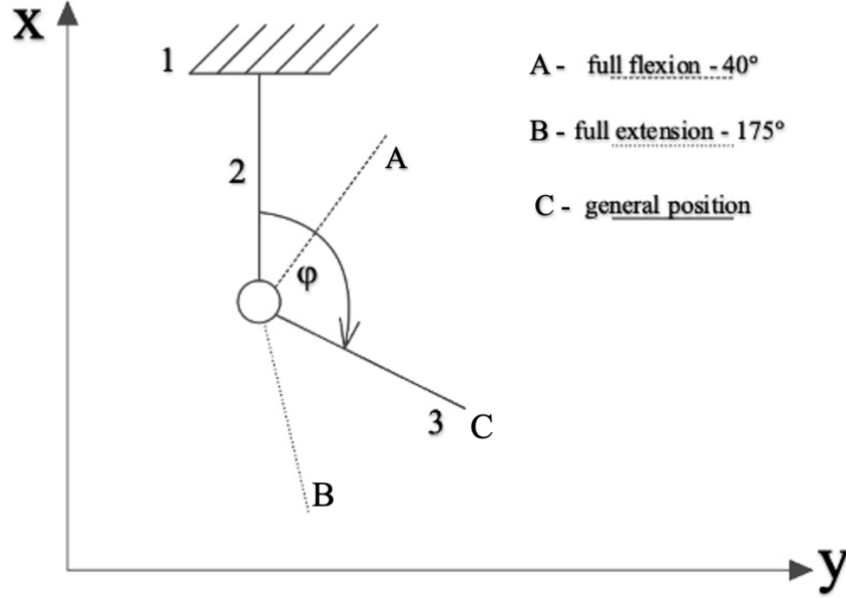


Figure 30: Geometry of the upper arm. 1- frame, 2-upperarm, 3-forearm with hand, A- full flexion, B- full extension, C- general position.

We consider cyclic motion with one time period which consists of flexion at first and then extension. Range of motion is chosen $\varphi \in \langle 40^\circ ; 175^\circ \rangle$ where 40° corresponds to full flexion and 175° corresponds to full extension. The angle φ is a function of the time. Time period is chosen as 2s and time step is 0.02s, resulting 101-time steps. The elbow motion is defined as a harmonic function with a cosine waveform:

$$\varphi(t) = \varphi_m + \varphi_a \cos(\omega t) \quad (4)$$

$$\varphi(t) = \frac{\varphi_{max} + \varphi_{min}}{2} + \frac{\varphi_{max} - \varphi_{min}}{2} \cos(\omega t) \quad (5)$$

Because we solve the problem as a quasistatic where the moving segments are considered almost static, i.e their motion is slow, we can use static methods and equations for solving the issue. To determine optimized force of each muscle is necessary to define the static equilibrium of the elbow joint. This has the effect of ignoring the dynamic elements whereby we can describe static equilibrium of the elbow joint using moment equations of equilibrium:

$$\vec{M}_V = \vec{r}_i \times \vec{F}_i \quad (6)$$

where M_V is torque vector generated by a force of gravity, \vec{F} is a vector of muscle forces and \vec{r}_i is matrix of moment arm. The release forearm in the general position is shown in Fig. 31.

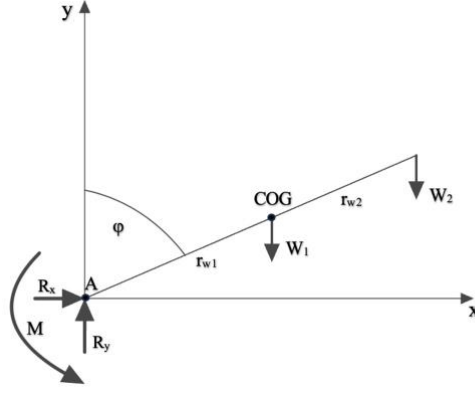


Figure 31: Release of the forearm in general position

$$M - W_1 r_{w1} \sin \varphi + W_2 (r_{w2} + r_{w1}) = 0 \quad (7)$$

The force torque generated by each muscle can be expressed as follows:

$$M = \sum_{i=1}^{n=7} \vec{M}_{Mi} = \sum_{i=1}^{n=7} \vec{r}_i \times \vec{F}_i \quad (8)$$

$$\vec{M}_{Mi} = f_i (\vec{e}_i \times \vec{r}_i) \quad (9)$$

where f is scalar value of muscle force, e is the unit vector and r is the moment arm. The unit vector is calculated using the following equation:

$$\vec{e} = \frac{\vec{r}_D - \vec{r}_P}{|\vec{r}_D - \vec{r}_P|} \quad (10)$$

Because the forearm is rotating around point A (Fig. 32), the distal attachments of coordinate system 1 are transformed by the equation:

$${}^2\vec{r}_D = \bar{R} {}^1\vec{r}_D \quad (11)$$

where R is the rotation matrix with following shape:

$$\bar{R} = \begin{bmatrix} \cos \varphi & \sin \varphi \\ -\sin \varphi & \cos \varphi \end{bmatrix} \quad (12)$$

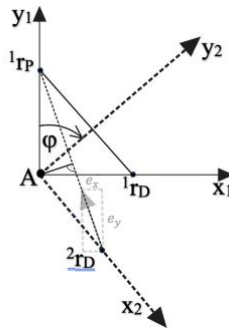


Figure 32: Rotating of coordinate system 2

4.1.2 Input Data

At first, here will be describe calculating weights and centres of gravity of each segment. These parameters are computed for the male human body with a weight of 80 kg, height of 180 cm, forearm length of 30 cm, hand length of 20 cm and varying weight in the hand. The calculation parameters of these parameters can be done according to the following regressive equation [37]:

$$y = b_0 + b_1 x_1 + b_2 x_2 \quad (13)$$

where is

y	individual computing parameter of segment
x_1	weight of human body [kg]
x_2	height of human body [cm]
b_i	experimental measured coefficient (Tab. 2)

segment weight [kg]			
	b_0	b_1	b_2
forearm	0.3185	0.01445	-0.00114
hand	-0.1165	0.0036	0.00175
position of the COG along the longitudinal axis [cm]			
forearm – styliion radiale	0.192	-0.028	0.093
hand – 3 rd dactylion	4.11	0.026	0.033

Table 2: Coefficients for forearm and hand [37]

The relevant parameters are calculated using the aforementioned coefficients and relations (Tab. 3).

i -segment	weight [kg]	position of the COG [m]	W_i [N]	r_{wi} [m]
1-forearm	1.27	0.147	12.46	0.153
2-hand	0.49 (+variable weight)	0.121	4.86	0.227

Table 3: Parameters of the forearm and the hand

Other important inputs data includes the proximal and distal attachments of each muscle. The proximal attachment is located on the humerus, and the distal attachment is located on the forearm. These attachments are presented in Tab. 4 in the form of $[x ; y]$. In this Table 4 is also shown maximal isometric force F_0^M , optimal fibre length L_0^M and pennation angle α . The data was imported from the OpenSim software from the DAS musculoskeletal model developed by Chadwick et. al [39].

	Name	$F_0^M [N]$	$L_0^M [N]$	$\alpha [rad]$	$r_P [m]$	$r_D [m]$
1	BRD	82	0.2756	0	[0;0.06]	[0;0.26]
2	BIClon	347	0.3154	0	[0;0.3]	[0;0.06]
3	BICbre	322	0.3055	0	[0;0.29]	[0;0.06]
4	BRA	314	0.1388	0	[0;0.12]	[0;0.057]
5	TRImed	263	0.1769	0.2967	[0;0.15]	[0;0.02]
6	TRIlnt	410	0.2465	0.0870	[0;0.22]	[0;0.02]
7	TRIlon	327	0.3263	0	[0;0.30]	[0;0.02]

Table 4: Parameters of Muscles

4.1.3 Optimization

This chapter describe the optimization methods of solving muscle redundancy. In our scenario, we deal with a quasistatic inverse kinematics problem, when the motion of the mechanism and the external forces are known, and we are looking for the resulting muscular propulsion effects.

No. Opt.	Objective function	Subject to	Boundaries	Initial condition
1	$G_1 = \min \sum_{i=1}^{n=7} F_i^2$	$M = \sum_{i=1}^{n=7} r_i F_i$	$F_i \in \langle 0 ; F_{0i}^M \rangle$	$F_{0i}^M * 0.01$
2	$G_2 = \min \sum_{i=1}^{n=7} a_i^2$	$M = \sum_{i=1}^{n=7} r_i F_i^M$	$a_i \in \langle 0 ; 1 \rangle$	$F_{0i}^M * 0.01$

Table 5: Parameters of optimization

When we have all the required input variables (moment of elbow joint and muscle moment arms) for eq. 8, we can proceed with the optimization of our unknown variables. In this phase, we decided to minimize the objective functions shown in Tab. 5. We solve muscle redundancy problem both without (No. Opt .1) and with the Hill type muscle model (No. Opt .2).

4.1.4 Hill Type Muscle Model in Optimization

To achieve a more realistic view of our problem, we used the Hill type muscle model (Fig. 33). The total muscle force is computed using eq. 1. For better overview, it is written below again [22]:

$$F^M = F_0^M (f_L^{active} f_v a(t) + f_L^{passive}) \cos(\alpha)$$

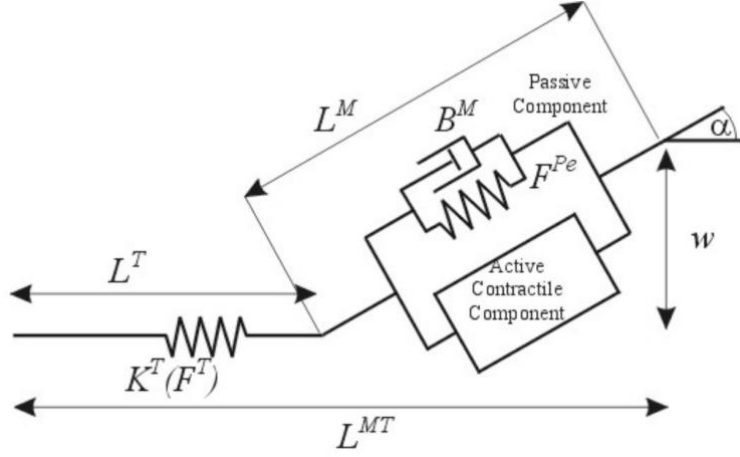


Figure 33: Hill type muscle model [20]

Then, the objective function G_2 has subject to:

$$M = \sum_{i=1}^{n=7} F_{0i}^M f_{Li}^{passive} \cos(\alpha_i) r_i + \sum_{i=1}^{n=7} F_{0i}^M f_{Li}^{active} f_{vi} \cos(\alpha_i) a_i r_i \quad (14)$$

The variables mentioned in the equation above are explained below. The equation for the active force-length relation of the muscle is computed as follows [22]:

$$f_L^{active} = 1 - \left[\frac{\left(\frac{L^M}{L_0^M} - 1 \right)^2}{0.5} \right] \quad (15)$$

where L^M is the actual muscle fibre length and L_0^M is the optimal muscle fibre length. The passive force-length of the muscle is computed as follows [22]:

$$f_L^{passive} = \left(\frac{L^M}{L_0^M} \right)^3 \exp \left[8 \frac{L^M}{L_0^M} - 12.9 \right] \quad (16)$$

The relationship between muscle force and contraction velocity for eccentric contraction is calculated using the following equation [22]:

$$f_v = \frac{2 v_0^M - b' + v^M \frac{a'}{F_0^M}}{v_0^M - b'} \quad (17)$$

where is

v^M	actual shortening/elongation velocity, $v^M = \dot{L}^M$
v_0^M	maximal velocity of shortening/elongation velocity, equal to $v_0^M = \frac{L_0^M}{0.1}$
a'	constant equal to $-0.284 F_0^M$ [23]
b'	constant equal to 11.51 mm/s [23]

And for isometric contraction, the relationship is defined by equation [22]:

$$f_v = \frac{v_0^M - v^M}{v_0^M + c v^M}, \quad (18)$$

where $c=4$ is a constant. Additional relations are defined below to calculate all the mentioned variables. The first one is the maximal isometric force of the muscle, which is defined as follows [20]:

$$F_0^M = PCSA \sigma \quad (19)$$

where $PCSA$ is the physiological cross-sectional area of the muscle and σ is the specific muscle tension $\in \langle 10, 51 \rangle \text{ Ncm}^{-2}$ [24]. The second relation is for the pennation angle, which is defined as follows [22]:

$$\alpha = \cot^{-1} \left[\frac{L_0^M \sin \alpha_0}{L^{MT} - L_S^T} \right] \quad (20)$$

where L_S^T is the tendon slack length, α_0 is the pennation angle at optimal fibre length and L^{MT} is the total length of the musculotendon complex:

$$L^{MT} = L^T + L^M \cos \alpha \quad (21)$$

4.2 Muscle Force Assessment through Outputs

Once we have obtained the necessary outputs (moment of elbow joint and muscle moment arms) from the chapter 4.1., we can create and implement proprioception models which are based on the musculoskeletal model defined in the previous chapter. These models are founded on a common optimization criterion:

- *Regulating muscle activity to achieve the minimum overall signal to the CNS from GTOs.*

The concept of this chapter is to introduce GTO models, from simple to more difficult. We solve implementation of proprioception in the musculoskeletal model both without and with the Hill type muscle model, similar to 4.1.

GTOs are force sensitive proprioceptors. We consider that GTOs could be important for regulating muscle activity by the CNS. For this reason, we only deal with GTOs within these models and do not include muscle spindle models.

4.2.1 Linear Model

In this model we assume that the GTOs are ideal force generator and the output signal from GTOs is proportional to the muscle force. The output signal from GTOs for the entire muscle is proportional, because the total muscle force is proportional to the number of activated motor unit. Additionally, we consider that as the muscle force increases and more GTOs are activated, the afferent signal also increases. Our objective is to minimize the total output signal G for the entire motion:

$$G = \sum_{i=1}^{n=7} \lambda_i F_i \quad (22)$$

where λ_i are the weights of each muscle force F_i . These weights can be expressed as the number of GTOs in each muscle:

$$\lambda_i = N_{GTOi} \quad (23)$$

Since the number of GTOs in muscles is less unknown than the number of MSs [41], we operate on the assumption that in muscle is about 80% of GTO as MSs [40].

$$N_{GTOi} = 0.8 \rho_{MSi} m_i \quad (24)$$

where ρ_{MSi} is the density of MS of i -th muscle and m_i is the mass of i -th muscle, that can be expressed as follows:

$$m_i = \rho_{muscle} l_{0i} PCSA_i \quad (25)$$

where ρ_{muscle} is the density of muscle, l_{0i} is its resting length and $PCSA_i$ is its physiological cross-sectional area. The density of MS of i -th muscle can be expressed as follows [42]:

$$\rho_{MSi} = 20.5 m_i^{0.49} \quad (26)$$

Then the output signal G can be expressed as follows:

$$G = \sum_{i=1}^{n=7} 0.8 \rho_{MSi} m_i F_i \quad (27)$$

where ρ_{MSi}, m_i are known values and F_i are unknown values. Then the output signal G with considering the Hill type muscle model can be expressed as follows:

$$G = \sum_{i=1}^{n=7} 0.8 \rho_{MSi} m_i F_0^M (f_L^{active} f_v a(t) + f_L^{passive}) \cos(\alpha) \quad (28)$$

4.2.2 Variability Model

The initial model we chose for the linear model comparison is based on the standard deviation of the force from each muscle. Standard deviation is a statistical measure that indicates how much the individual numbers in a dataset are spread out around the mean value. If the values are closer to the mean, the standard deviation will be lower, which means less variability in the data. Conversely, if the values are more spread out from the mean, the standard deviation will be higher. The modified formula for calculating the standard deviation in our context is (K represents the no. time steps):

$$G = \sqrt{\frac{1}{K-1} \sum_{i=1}^{n=7} (F_i - \bar{F}_i)^2} \quad (29)$$

When we want to include the Hill type muscle model into the formula for calculating standard deviation, the formula becomes:

$$G = \sqrt{\frac{1}{K-1} \sum_{i=1}^{n=7} (a_i - \bar{a}_i)^2} \quad (30)$$

4.2.3 Lin and Crago Model

The second model we chose for the linear model comparison was developed by Lin and Crago (2002) [27]. They approximated the nonlinear behaviour of the GTO as a muscle force sensor using the following formulation:

$$G = \sum_{i=1}^{n=7} r_i N_{GTOi} \quad (31)$$

where r_i represents the response of one GTO:

$$r_i = A \ln\left(\frac{F_{1i}}{B} + 1\right) \quad (32)$$

where A, B are constants with values $A= 60 \text{ impulses/s}$ and $B= 4 \text{ N}$. The Force F_{1i} from a single muscle fascicle is calculated as follows:

$$F_{1i} = \frac{F_i}{N_{GTOi}} \quad (34)$$

where F_i is the force of i -th muscle and N_{GTOi} is the number of GTOs of i -th muscle, which is defined in eq. (24). This relationship is based on the assumption that the total force from each muscle equals the sum of the forces from all muscle fascicles, and that a single GTO senses the force from a muscle fascicle. Additionally, we assume uniform activation of muscle fibres within each muscle. Then the output signal G with and without the Hill type muscle model can be expressed on the base on the same principle as described in chapter 4.2.1.

4.2.4 Hill-Langmuir Model

For the third model we selected Hill-Langmuir equation, which is especially used in biochemistry. In general, the Hill equation itself reflects the tissue response to the physiological output of the system, such as muscle contraction. The Hill-Langmuir equation is a special case of a rectangular hyperbola which can be expressed without Hill type muscle model as follows:

$$G = \sum_{i=1}^{n=7} \frac{1}{1 + \left(\frac{1}{2F_i}\right)^k} \quad (35)$$

where F represents the force of muscle and k is the Hill coefficient. If we want to include the Hill type muscle model, the function becomes:

$$G = \sum_{i=1}^{n=7} \frac{1}{1 + \left(\frac{1}{2a_i}\right)^k} \quad (36)$$

The outcomes of these functions generate sigmoidal curves (Fig. 34). In our case represent respond of muscle activation.

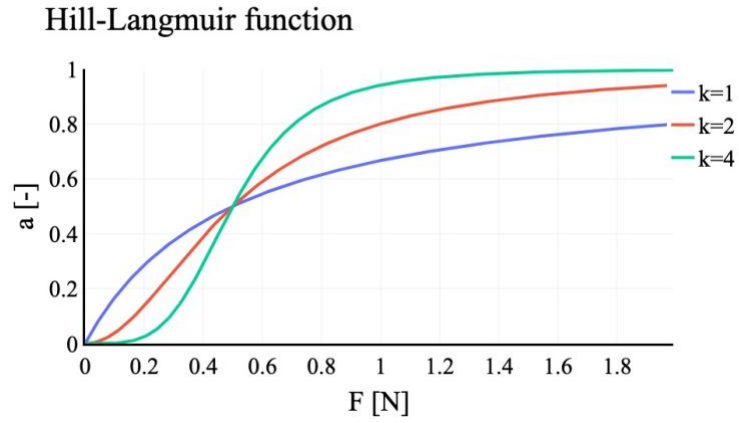


Figure 34: Curves dependent on coefficient k , where $k=1$ is red curve, $k=2$ is orange curve, and $k=4$ is purple curve

One of our specific objectives is to integrate proprioception into the musculoskeletal model. Our emphasis is on Golgi tendon organs (GTOs), which are situated within the muscle tendon. Tendons display non-linear elastic behaviour, characterized by a curve similar to the one shown in Fig. 34 for $k=4$. It appears that an appropriate choice for the Hill coefficient would be $k=4$.

4.2.5 Input Data and Optimization

Muscle weight and the calculated density of muscle spindles (MSs) for each muscle are presented in Tab. 6 [42].

	Name	m_i [g]	ρ_{MSi} [–]
1	BRD	67.4	161.4
2	BIClon	82.8	177.63
3	BICbre	82.8	177.63
4	BRA	141	231.7
5	TRImed	92.5	188.4
6	TRIlal	94.2	190.1
7	TRIlon	138.4	229.6

Table 6 Weight and density of MSs of i -th muscle

The optimization methods of solving implementation of proprioception to the musculoskeletal model are presented below (Tab. 7):

No. Opt.	Objective function	Subject to	Boundaries	Initial condition
3	$G_3 = \min \sum_{i=1}^{n=7} \lambda_i F_i$	$M = \sum_{i=1}^{n=7} r_i F_i$	$F_i \in \langle 0 ; F_{0i}^M \rangle$	$F_{0i}^M * 0.001$
4	$G_4 = \min \sum_{i=1}^{n=7} \lambda_i F_i^M$	$M = \sum_{i=1}^{n=7} r_i F_i^M$	$a_i \in \langle 0 ; 1 \rangle$	
5	$G_5 = \min \sum_{i=1}^{n=7} r_i N_{GTOi}$	$M = \sum_{i=1}^{n=7} r_i F_i$	$F_i \in \langle 0 ; F_{0i}^M \rangle$	
6	$G_6 = \min \sum_{i=1}^{n=7} r_i N_{GTOi}$	$M = \sum_{i=1}^{n=7} r_i F_i^M$	$a_i \in \langle 0 ; 1 \rangle$	
7	$G_7 = \sqrt{\frac{1}{K-1} \sum_{i=1}^{n=7} (a_i - \bar{a}_i)^2}$	$M = \sum_{i=1}^{n=7} r_i F_i^M$	$a_i \in \langle 0 ; 1 \rangle$	
8	$G_8 = \sqrt{\frac{1}{K-1} \sum_{i=1}^{n=7} (F_i - \bar{F}_i)^2}$	$M = \sum_{i=1}^{n=7} r_i F_i$	$F_i \in \langle 0 ; F_{0i}^M \rangle$	
9	$G_9 = \min \sum_{i=1}^{n=7} \frac{1}{1 + (\frac{1}{2 F_i})^k}$	$M = \sum_{i=1}^{n=7} r_i F_i$	$F_i \in \langle 0 ; F_{0i}^M \rangle$	
10	$G_{10} = \min \sum_{i=1}^{n=7} \frac{1}{1 + (\frac{1}{2 a_i})^k}$	$M = \sum_{i=1}^{n=7} r_i F_i^M$	$a_i \in \langle 0 ; 1 \rangle$	

Table 7: Parameters of optimization

4.3 Golgi Tendon Organ Distribution

In this section, we do dual optimization (Tab. 8) whose result are unique values of density of GTOs for each muscle ρ_{GTOi} . For this optimization process we decided to use objective function G_{10} , which represents the Hill-Langmuir equation with the Hill type muscle model. Initially, we optimize the activation of each muscle a_i during each time step.

No. Opt.	Objective function	Subject to	Boundaries
11	$G_{11} = \min \sum_j^p \sum_i^n \frac{1}{1 + \left(\frac{1}{2a_{ij}}\right)^k} \rho_{GTOij}$ <p>$i=1,...,7$ (muscles) and $j=t_0,..., t_{end}$</p>	$M = \sum_j^p \sum_i^n r_i F_i^M$ $\sum_{i=1}^{n=7} \rho_{GTOi} = 1$	$a_i \in \langle 0 ; 1 \rangle$ $\rho_{MSi} \in \langle 0.1 ; 1 \rangle$
12	$G_{12} = \min \sum_{i=1}^{n=7} \frac{1}{1 + \left(\frac{1}{2a_i}\right)^k} \rho_{GTOi}$	$M = \sum_{i=1}^{n=7} r_i F_i^M$	$a_i \in \langle 0 ; 1 \rangle$ $\rho_{MSi} \in \langle 0.1 ; 1 \rangle$

Table 8: Optimization criteria for GTO distribution

This optimization yields an optimal set of GTO densities for each muscle ρ_{GTOi} across the entire motion. These ρ_{GTOi} densities are used as inputs for the second optimization, which uses the objective function G_{12} to optimize the activation of each muscle for each time step during the elbow motion. Following that, we obtain the ideal densities ρ_{GTOi} for each muscle during elbow motion, as well as a single optimal value of G_{12} representing the resulting output signal.

5 Results

The resulting muscle load were obtained by optimizing the selected functions $G_{l=1,...,12}$ with appropriate constraints. The results are presented for a musculoskeletal model with 7 muscles performing motion at the elbow joint. The calculated optimizations are based on both linear and nonlinear models, which are compared with each other. The results are divided into four distinct sections. In section **5.1.** is shown muscle force assessment through inputs, in **5.2.** is presented muscle force assessment through outputs, in **5.3.** are presented the results of GTO distribution and in **5.4.** are presented the optimized activations of selected models. All of the results are calculated for four variations: with and without the utilization of the Hill-type muscle model, and with and without the addition of a 2.5 kg weight in hand. The objective functions with the inclusion of the Hill type muscle model are G_2 , G_4 , G_6 , G_7 and G_{10} . The objective functions without the Hill type muscle model are G_1 , G_3 , G_5 , G_8 and G_9 . Abbreviations are used to describe the muscles in the text: BRD (m. brachioradialis), BIClon (m. biceps longus), BICbre (m. biceps brevis), BRA (m. brachialis), TRImed (m. triceps medialis), TRIlat (m. triceps lateralis) and TRIlon (m. triceps longus).

The following graphs show the loading in individual muscles throughout the course of elbow motion. The motion begins from a state of full extension ($t=0s$), with the arm in a position along the body. Then the forearm moves into a state of full flexion ($t=1s$) and ends up in full extension again ($t=2s$). Each figure presents results for two distinct variations:

- On the *left* is always variation *without* the addition of weight in hand.
- On the *right* is always variation *with* the addition of 2.5 kg weight in hand.

5.1 Optimized Inputs

In Fig. 35, it can be seen that loading in individual muscles has the same course in both cases, with and without added weight in hand. In this case, only flexors are activated, and extensors show no activation during the entire motion. *BRD* load progression has less variance than the rest of the flexors. *BRD*, *BIClon* and *BICbre* have a similar level of loading during the entire motion.

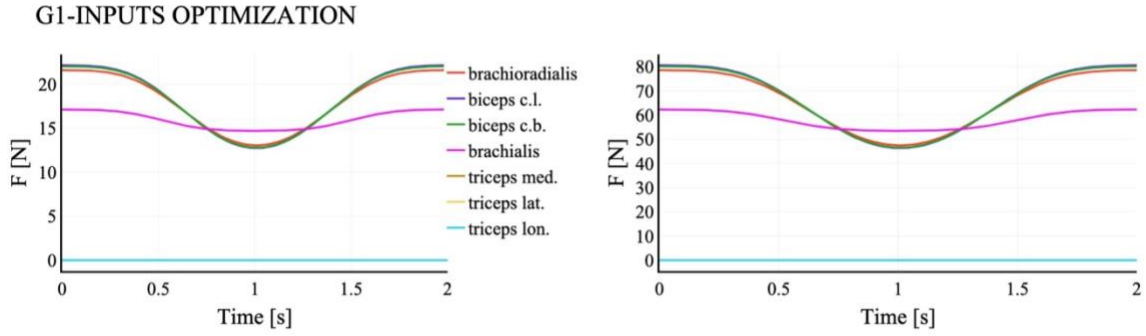


Figure 35: Optimized loading in individual muscles with G_1 objective function. (Left - w.o. added weight in hand. Right-w. added weight in hand).

If we include the Hill type muscle model into the same objective function, the loading in individual muscles changes significantly (Fig. 36). In this model, we can see that *BRD* activity is minimal in both cases (with and without added weight), as are the extensors. Compared to the G_1 function, *BRA* load progression has more variance than both heads of the m. biceps brachii. When the forearm reaches the full flexion position, *BRA* exhibits a significant decrease in loading and then its loading increases.

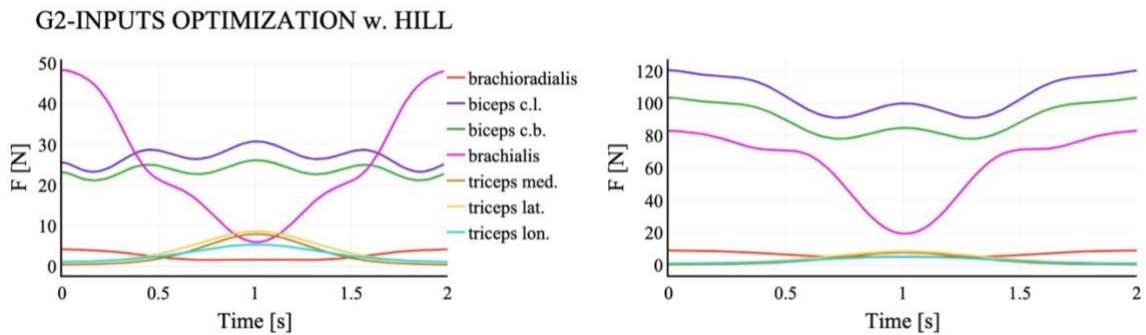


Figure 36: Optimized loading in individual muscles with G_2 objective function. (Left - w.o. added weight in hand. Right-w. added weight in hand).

5.2 Optimized Outputs

In this chapter, the results of optimized outputs are shown as muscle force assessment with the implementation of proprioception to the musculoskeletal model, both without and with the Hill type muscle model. At first, we used a linear proprioception model that represent the G_3 and G_4 objective function. In Fig. 37, it can be seen a common principle: during all or parts of the elbow motion, only one muscle is activated. In the case without added weight, only *BRD* is activated at or close to its maximum isometric force 82 N. On the other hand, with added weight, *BIClon* is mainly active and then, in area of full flexion position, is mainly active *BICbre* and then *BIClon* again. *BRD* is active at the same level throughout the motion. In both cases (with and without added weight), flexors and *BRA* show no activation.

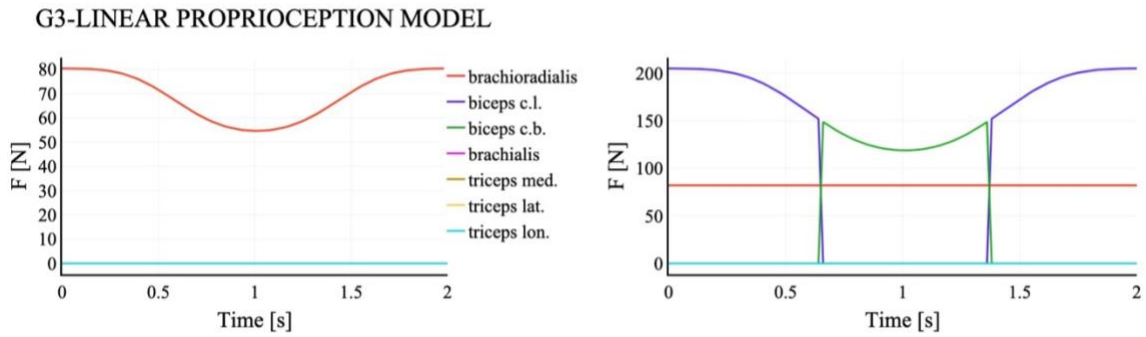


Figure 37: Optimized loading in individual muscles with G_3 objective function. (Left - w.o. added weight in hand. Right-w. added weight in hand).

When we insert the Hill type muscle model into the same objective function, the loading in individual muscles shows to some extent the same principle as in the previous case (Fig. 38). In the case without added weight, we can see load *BRD*, *BRA*, *BICbre*, *BIClon* at the beginning as same as at the end of the motion. The main part of the elbow motion activates only *BRD*. In the case with added weight, *BIClon*, *BICbre* and *BRD* are active like in the previous Fig. 37.

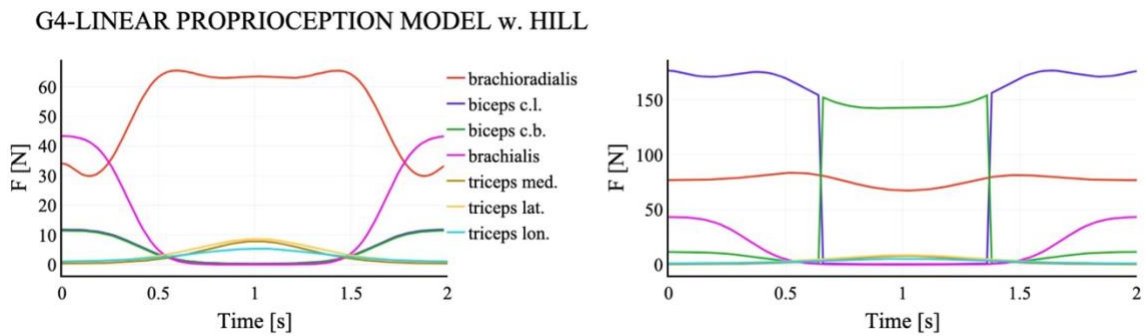


Figure 38: Optimized loading in individual muscles with G_4 objective function. (Left - w.o. added weight in hand. Right-w. added weight in hand).

If we use nonlinear model by Lin and Crago without the Hill type muscle model (Fig. 39), it can be seen same course of loading in individual muscles as in the G_3 function. In the case without added weight, the loading course is even exactly the same, and in the case with added weight, the pattern of *BIClon* and *BICbre* remains the same. The only difference is the absence of active BRD as shown in Fig. 37.

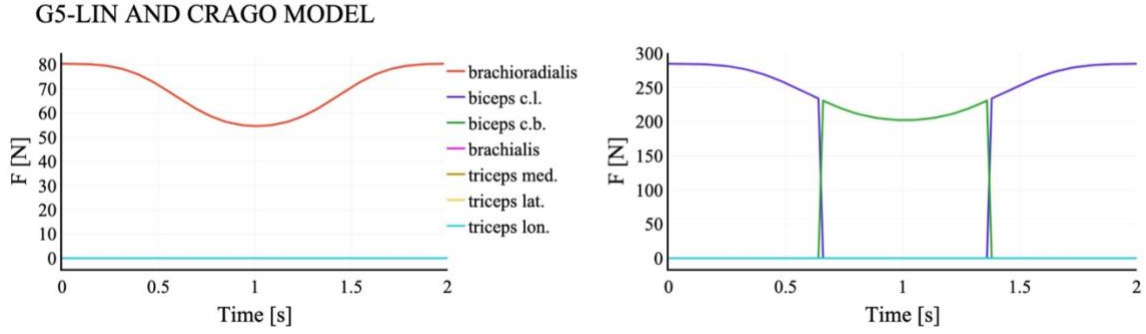


Figure 39: Optimized loading in individual muscles with G_5 objective function. (Left - w.o. added weight in hand. Right-w. added weight in hand).

The Lin and Crago model with the Hill type muscle model exhibits similar features to the G_4 function (Fig. 40). In the case without added weight, the curves have the same shape, but now *BIClon* is primarily loaded. Similarly, in the case with added weight, loading is carried only by *BIClon*.

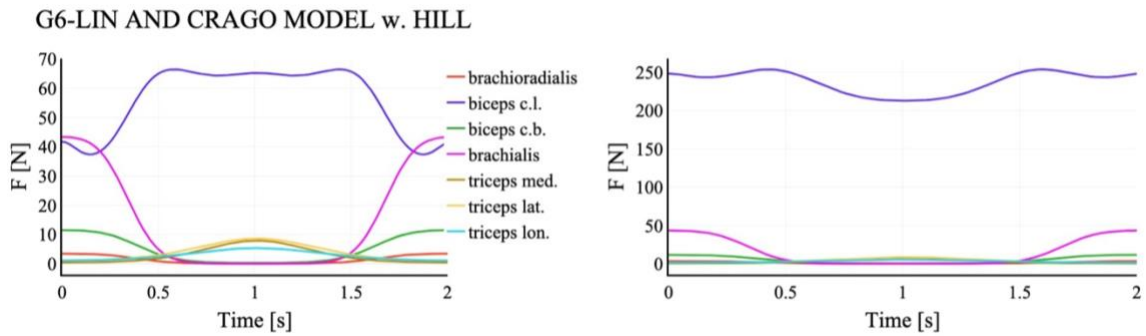


Figure 40: Optimized loading in individual muscles with G_6 objective function. (Left - w.o. added weight in hand. Right-w. added weight in hand).

The third nonlinear model is the variability model with the Hill type muscle model, representing objective function G_7 (Fig. 41). In both cases (with and without added weight), we observe the same pattern of waveforms. We can see peaks of muscle load during flexion as well as in extension. In the middle of the motion, the loading of all extensors increases, and conversely, the loading of *BRA* decreases.

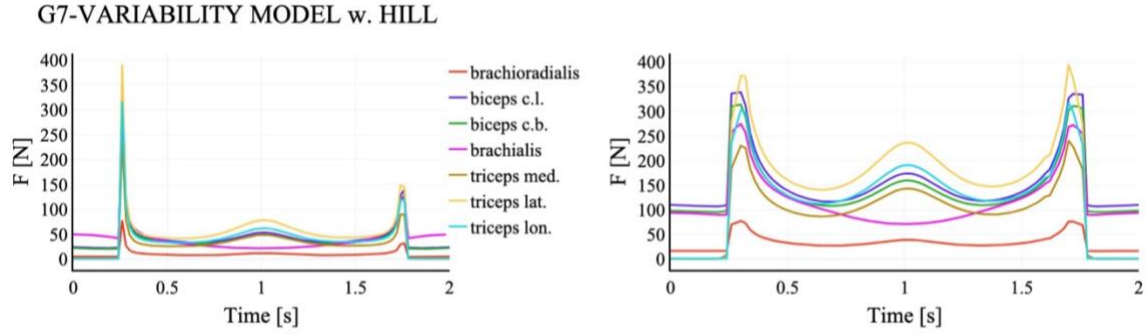


Figure 41: Optimized loading in individual muscles with G_7 objective function. (Left - w.o. added weight in hand. Right-w. added weight in hand).

The variability model without the Hill type muscle model provides us with more interesting results (Fig. 42). Here, we observe peaks of muscle load at the beginning as well as at the end of the motion. But in the middle of the motion, all muscles exhibit the same level of loading. In the case without the Hill model, this pattern persists for 1.5 s, whereas in the case with the Hill model, it persists for almost 1 s.

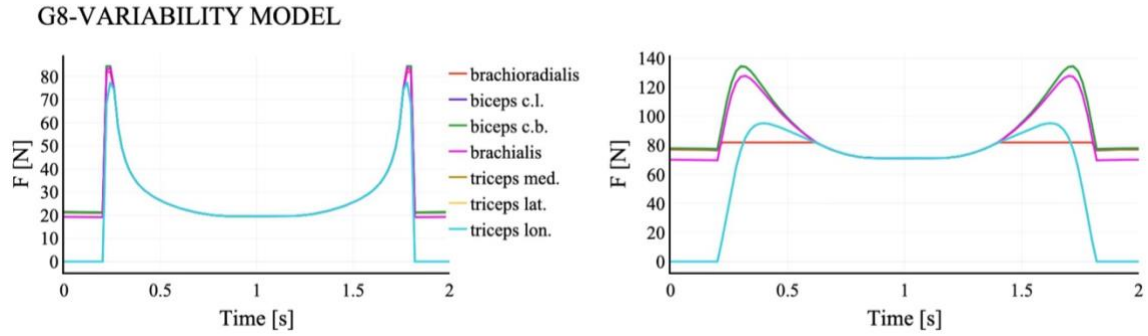


Figure 42: Optimized loading in individual muscles with G_8 objective function. (Left - w.o. added weight in hand. Right-w. added weight in hand).

The last model is the Hill-Langmuir model, which represents objective function G_9 (without the Hill model) and G_{10} (with the Hill model). In Fig. 43 (without the Hill model), it can be seen that the loading in all muscles follows a similar course in both cases, with and without the added weight in the hand, similar to the function G_1 . The difference lies in BRA . In both cases (with and without the added weight), BRA exhibits a lower level of loading than the rest of the flexors. All extensors show no activity during the entire elbow motion.

G9-HILL-LANGMUIR MODEL

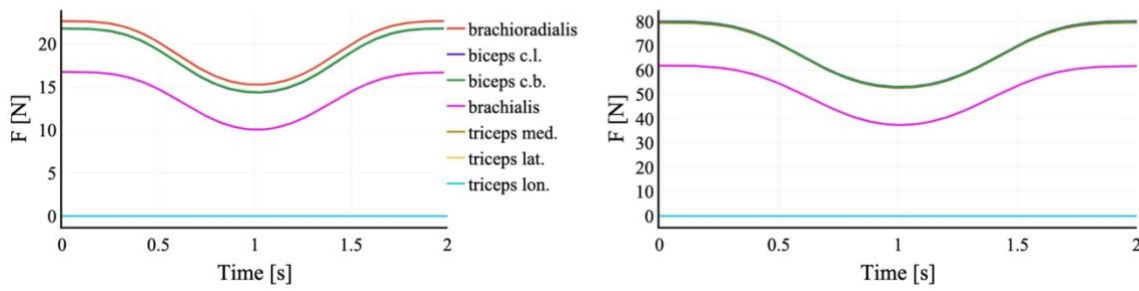


Figure 43: Optimized loading in individual muscles with G_9 objective function. (Left - w.o. added weight in hand. Right-w. added weight in hand).

If we include the Hill type muscle model into the Hill-Langmuir model, the loading in individual muscles changes significantly (Fig. 44). Similarly, all muscles show a similar pattern of waveform as in function G_2 . We can observe that *BRD* loading is minimal in both cases (with and without added weight), similar to extensors. *BRA* load progression has more variance compared to *BICbre* and *BIClon*. When we want to compare G_{10} with G_9 , we can observe a different course for *BRA*. The musculus brachialis exhibits a significant decrease in loading when the forearm reaches the full flexion position.

G10-HILL-LANGMUIR MODEL w. HILL

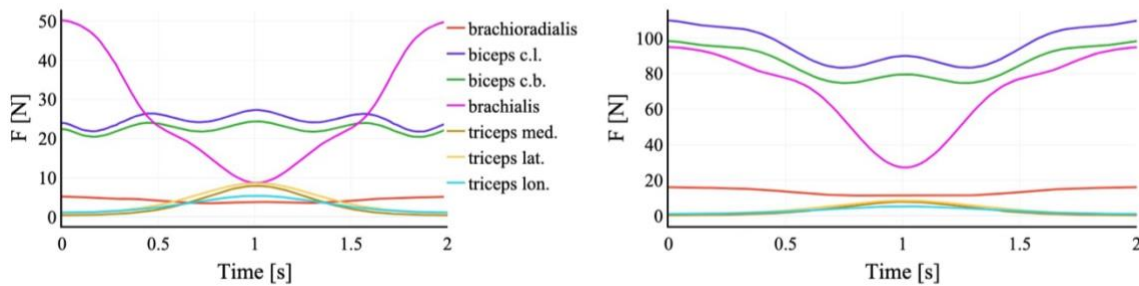


Figure 44: Optimized loading in individual muscles with G_{10} objective function. (Left - w.o. added weight in hand. Right-w. added weight in hand).

5.3 Golgi Tendon Organ Distribution

In this chapter, the results of the dual optimization of objective function G_{11} , respectively G_{12} with the implemented Hill type muscle model are presented. The first set of graphs in Fig. 45 is for a Hill coefficient equal to $k=4$. The second set of graphs in Fig. 46 is for $k=2$.

In Fig. 45, we can see that *BRA*, *BIClon* and *BICbre* start at different levels of loading in the case without added weight. Then both heads of the biceps brachii exhibit a gradual convergence to a similar value of loading. Loading of *BRA* decreases during flexion and increase during extension. *BRA* shows a high level of loading throughout the entire motion. *BRD* with all extensors show a minimum level of loading. In the case with added weight, we can see that the main load is carried by *BIClon*, *BICbre* and *BRA*.

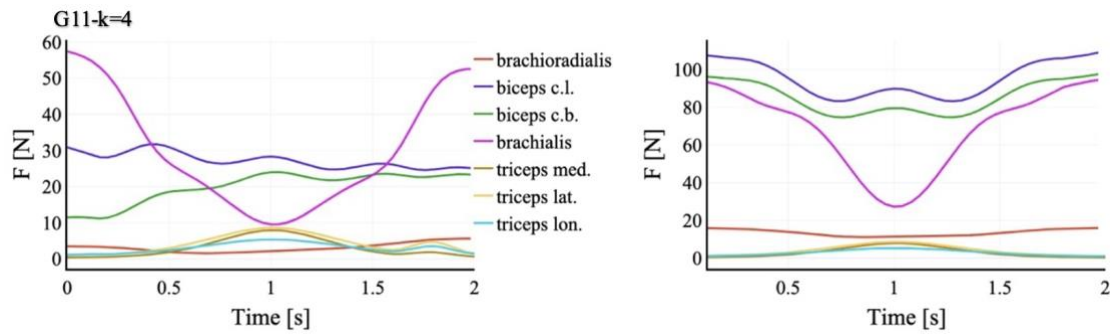


Figure 45: Optimized loading in individual muscles with G_{11} objective function, $k=4$. (Left - w.o. added weight in hand. Right-w. added weight in hand).

When we use a Hill coefficient equal to $k=2$, as shown in Fig. 46, in the case without added weight, we can observe that the loading of both biceps fluctuates around a single value throughout the entire motion. The loading course of *BRA*, *BRD* and the extensors follows the same pattern as in the previous case. In the case with added weight, the majority of loading is carried only by *BIClon*, while the rest of muscles show a minimum level of loading.

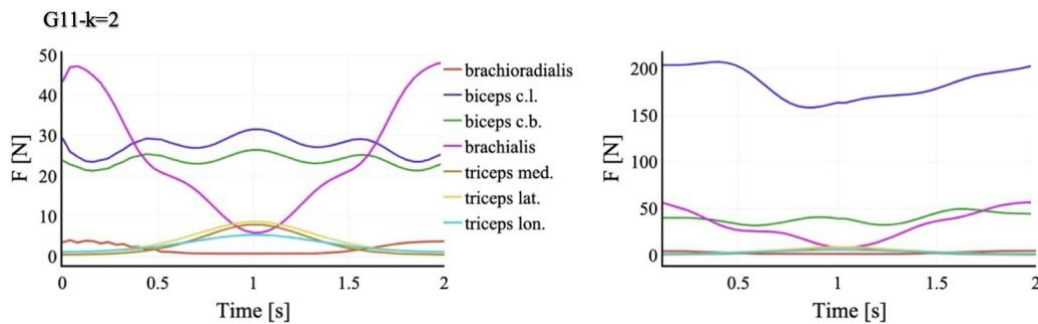


Figure 46: Optimized loading in individual muscles with G_{11} objective function, $k=2$. (Left - w.o. added weight in hand. Right-w. added weight in hand).

The calculated percentage representation of ρ_{GTOi} in each muscle during the elbow motion and the total output signal G_{12} are presented in Tab. 9 below:

	K=2, w.o. added weight in the hand	K=2, w. added weight of 2.5 kg in the hand	K=4, w.o. added weight in the hand	K=4, w. added weight of 2.5 kg in the hand
OUTPUT SIGNAL G_{12}	0.23	3.2	0.008	1.15
BRD	0.24	0.184	0.19	0.1
BIClon	0.1	0.1	0.17	0.1
BICbre	0.1	0.1	0.18	0.1
BRA	0.1	0.1	0.16	0.1
TRImed	0.15	0.11	0.1	0.1
TRIlnt	0.15	0.10	0.1	0.1
TRIlon	0.15	0.29	0.1	0.31

Table 9: Results of GTO optimization with using the Hill-Langmuir equation with the Hill type muscle model.

5.4 Course of Muscle Activation in Selected Models

This chapter presents the results of optimized activation in selected models. We chose the objective functions G_2 from optimized inputs, G_{10} from optimized outputs and both variations ($k=2$ and $k=4$) of G_{11} from Golgi Tendon Organ optimization.

In Fig. 47, in the case without added weight, we can see, that activation of flexors increases during flexion and then decreases during extension. In the case with added weight, the activation of flexors fluctuates around a single value throughout the entire motion. In both cases is the same pattern of activation level. The musculus biceps brachii has the highest activation level, followed by musculus brachialis, and then m. brachioradialis. Extensors are not activated during the entire motion.

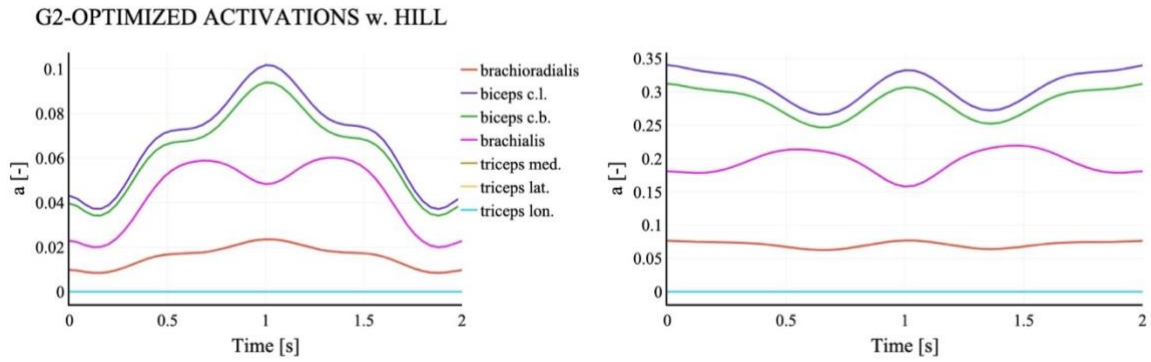


Figure 47: Optimized activations in individual muscles with G_2 objective function. (Left - w.o. added weight in hand. Right - w. added weight in hand).

In Fig. 48, a similar pattern to the previous figure is evident. However, there is one difference: BRD displays a higher level of activation than in the previous case. Additionally, all flexors exhibit a very similar course of activation.

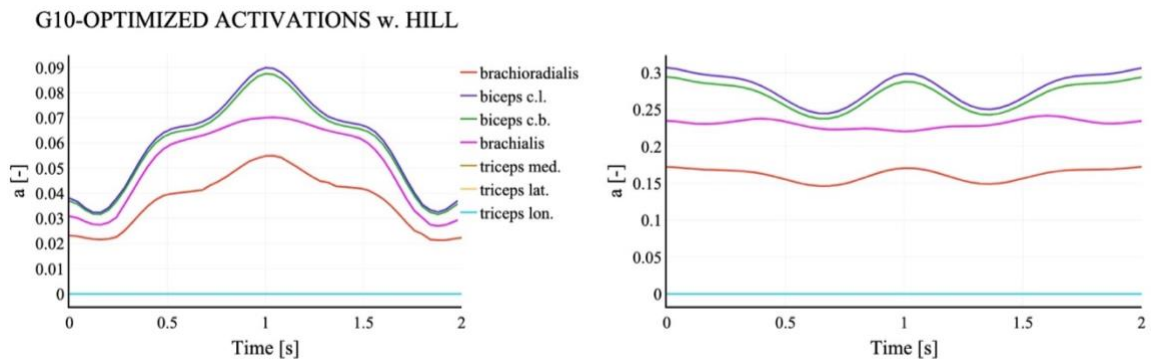


Figure 48: Optimized activations in individual muscles with G_{10} objective function. (Left - w.o. added weight in hand. Right - w. added weight in hand).

In Fig. 49, a slightly different course of activation in flexors can be observed in the case without added weight. Activation of *BICbre* starts from zero and then it goes up steeply. On the other hand, the rest of the flexors have a gradual increase in activation during flexion. Extensors have no activation almost the entire elbow motion. But at the end of the extension, we can see coactivation of extensors. In the case with added weight, the activation of each muscle fluctuates around a single value throughout the entire motion, similar to previous figures.

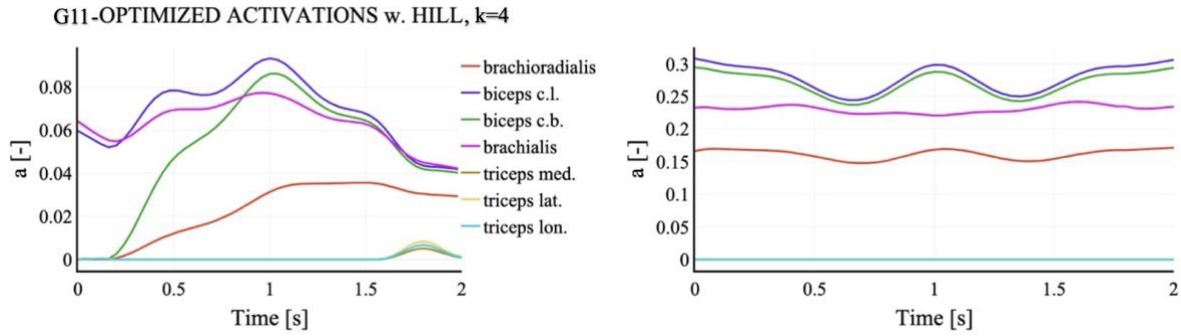


Figure 49: Optimized activations in individual muscles with G_{11} objective function, $k=4$. (Left - w.o. added weight in hand. Right-w. added weight in hand).

When we use a Hill coefficient equal to $k=2$ (Fig. 50), we can observe that in the case without added weight, the activation pattern of both biceps and *BRA* has the same patten during the entire motion. *BRD* demonstrates significant jumps at the beginning of flexion. In the case with added weight, we observe a higher level of activation of *BIClon* compared to the previous cases. Other flexors are activated at a minimum.

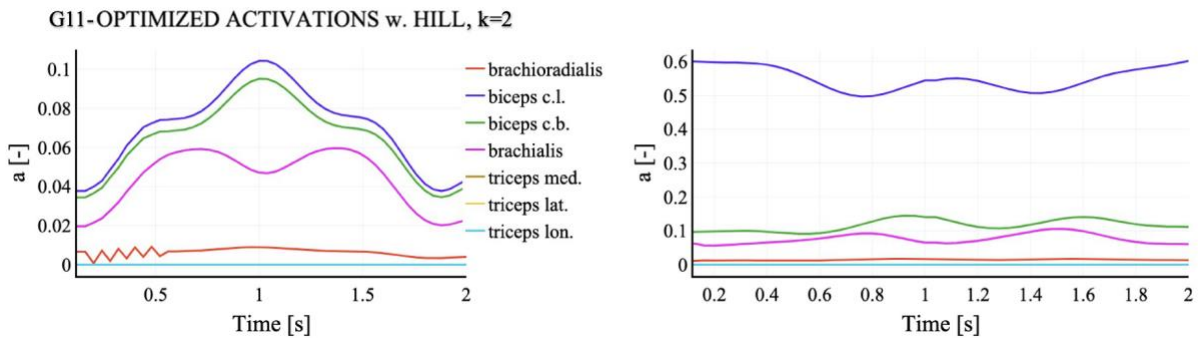


Figure 50: Optimized activations in individual muscles with G_{11} objective function, $k=2$. (Left - w.o. added weight in hand. Right-w. added weight in hand).

6 Discussion

We developed a 2D musculoskeletal model of the elbow joint. Subsequently, we demonstrated the solution of muscle redundancy through inputs optimization. We created and implemented a proprioception model based on Golgi tendon organs (GTOs) into the musculoskeletal model. We introduced several optimization criteria for this implementation. The outcomes obtained in this thesis are divided into four parts and are presented in Chapter 5. We varied the optimization criteria using simpler linear models to more complex nonlinear models. When comparing the obtained results, we observed different muscle behaviours between each model.

Differences between objective functions become evident when considering the utilization of the Hill type muscle model. Objective functions G_3 (Fig. 37), G_4 (Fig. 38), G_5 (Fig. 39), G_6 (Fig. 40), G_7 (Fig. 41) and G_8 (Fig. 42) give us inconsistent results that may be probably non-physiological. Interesting results shows function G_8 (Fig. 42) with variability model. We selected this model because, from a physiological point of view, we aim to create a model with minimal variability in loading/activation of muscles. All muscles exhibit a same level of loading during the elbow motion. This might be required in scenarios where we want to achieve a high level of elbow joint stiffness. Across the above-mentioned objective functions, we observe a common principle in muscle loading. It seems that in these cases, the brain tends to activate a single muscle and ignores the potential for distributing the load among other muscles. When we want to compare total output signal G_{12} (Tab. 9), we observe that we get better=lower value from GTO optimization with using the Hill-Langmuir equation with the Hill type muscle model with $k=4$ in both cases. Also, this variation gives us a more realistic percentage representation of ρ_{GTOi} in each muscle during the elbow motion.

The nervous system is a complex and sophisticated system. For this comparison, studies that deal with EMG measurements of muscles during movement at the elbow joint are selected. These studies could provide us with the necessary information to confirm or reject the stated hypothesis. If the stated hypothesis is confirmed, the selected models could be further modified and complexified to obtain results that correspond to reality. On the other hand, especially objective functions G_2 (Fig. 36) and G_{10} (Fig. 44) demonstrate results that approximate the real physiological situation relatively well. According to EMG findings, flexor activation rises during flexion and declines during extension, which is consistent with our model in Figure 49. When we compare the course of activation of the Hill-Langmuir model with the Hill type

muscle model with Hill coefficient $k=4$ (Fig. 49) to studies [44, 45, 46] in Fig. 25, 26 and 27, we can see a relative corresponding course of activation of *m. brachialis* and both heads of *m. biceps brachii* during flexion.

We certainly cannot claim that the more complex the model is, the more realistic results we get. Our model was created based on several simplifications. At first, we solved this issue quasistatically and in 2D. We have neglected dynamic force effects. There are also several input data that have a proportionally large variability e.g. maximum isometric force, density of muscle spindles, optimal fibre length, constants and coefficients. We must mention that we have chosen the SLSQP optimization method for this research, which is mainly used for searching local minimum (or maximum) of nonlinear functions. In general, local minimum search methods like SLSQP are susceptible to estimation of the initial conditions, and we can obtain very different results. The advantage of these methods is their computational speed. At this point we can speculate, which results we could obtain with global minimum search methods e.g. genetic algorithms.

One way to create a more detailed model that includes more aspects of this issue is by adding both Golgi tendon organs and muscle spindles to the musculoskeletal model. Another way to expand the model is by using a transfer function, which helps describe how nerve signals control muscle contractions and how muscles respond. Using this transfer function, we can better understand how nerves affect muscle movement and strength. This could help us improve how we model motion and analyze muscle responses.

Also related to this is the selection of the objective function, or the choice of the optimization criterion. Additionally, it should be noted that our form of optimization is basic, and we are not able to determine if the brain is optimizing motion in this way. The brain might employ alternative methods of activation during targeted or complex motion, which may not necessarily be optimal. We also cannot be sure that our presented optimization criteria have a physiological reason. For example, the utilization of the square of activation or the square of force is primarily used because they are well expressed mathematically, and they do not have great physiological importance. As a physiological criterium (designed by Crowninshield and Brand) is considered the sum of the cube of muscular stresses. This criterium minimize overall muscle fatigue [49]. But even here we do not know if it is physiological, because we do not know how the human

body works with the muscular stress. If we utilize the optimization criterium e.g. of force, it is up to us what exponent we choose.

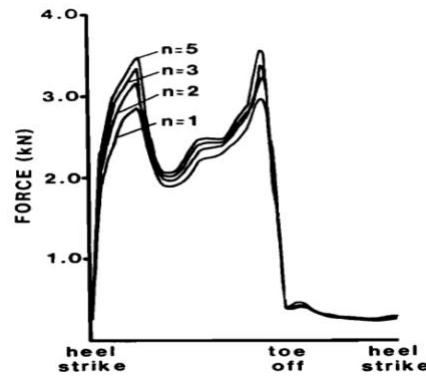


Figure 51: Differences in the muscle force predictions between linear and nonlinear criteria [47].

In Fig. 51 are shown differences in the muscle force predictions between linear and nonlinear with different degree of nonlinearity [47]. We observe that there is no fundamental difference between them. On the other hand, Raikova (1992) [48] reported that a global optimal criterion does not necessarily cover the physiological and the functional requirements of the body during motion. This can be true in the situation when the neural system has to accomplish more than one goal. The typical example is the task that requires high velocity and accuracy at time during the motion [47].

7 Conclusion

Within this study, we developed a musculoskeletal model of the elbow joint with implementation of proprioception. By employing various optimization criteria for proprioception, we were able to present muscle activity driven by proprioception. This study with all presented optimizations is freely available on GitHub website. A link to this thesis is provided in Appendix 1. Based on this research, we developed objective functions with specific optimization criteria that are close to the true physiological responses found in experimental studies. This allows us to investigate the following hypothesis:

“The optimal load for each muscle could be obtained by minimizing brain inputs from proprioceptors.”

Based on the findings presented in this paper, we confirm the above hypothesis. The present thesis provides a basis for a possible follow-up study, especially in terms of methodology and subsequent processing and evaluation of the obtained data. From a practical point of view, the work, in alignment with findings from other researchers, this study demonstrates the impact of muscle activity influenced by proprioception. Understanding muscular strategies during motor task allows the exploration of nervous system functioning. In terms of biomechanics, this knowledge provides information about physiological and mechanical requirements of a motor task across different daily or sport activities. The knowledge of muscle activation patterns can provide useful information for the understanding and prevention of injuries and the mechanisms that influence human body performance.

8 Sources

1. KITTNAR, Otomar. Lékařská fyziologie. Praha: Grada, 2011. ISBN 978-80-247-3068-4.
2. ČIHÁK, Radomír a Miloš GRIM. Anatomie 1. 2., uprav. a dopl. vyd. Ilustroval Milan MED. Praha: Grada Publishing, 2001. ISBN 80-7169-970-5.
3. DYLEVSKÝ, Ivan. *Funkční anatomie*. Praha: Grada, 2009. ISBN 978-80-247-3240-4.
4. BING. Pursuing Excellence: Structure and Function of the Muscular System (Part 1/2). *Pursuing Excellence*. Online. 19 May 2013. [Accessed 13 August 2023]. Available from: <http://michaelbingaman.blogspot.com/2013/05/growing-professionally-structure-and.html>
5. ČIHÁK, Radomír. *Anatomie*. Třetí, upravené a doplněné vydání. Ilustroval Ivan HELEKAL, ilustroval Jan KACVINSKÝ, ilustroval Stanislav MACHÁČEK. Praha: Grada, 2016. ISBN 978-80-247-5636-3.
6. pymuscle/docs/src/images/motor-unit-diagram.png at master · iandanforth/pymuscle. *GitHub*. Online. [Accessed 13 August 2023]. Available from: <https://github.com/iandanforth/pymuscle/blob/master/docs/src/images/motor-unit-diagram.png> A motor unit based model of skeletal muscle and fatigue-iandanforth/pymuscle
7. HOGERVORST, TOM M.D.†, AMSTERDAM, THE NETHERLANDS; BRAND, RICHARD A. M.D.‡, IOWA CITY, IOWA. Current Concepts Review - Mechanoreceptors in Joint Function*. The Journal of Bone & Joint Surgery 80(9):p 1365-1378, September 1998. <https://doi.org/10.2106/00004623-199809000-00018>
8. MILEUSNIC, Milana P. a Gerald E. LOEB. Mathematical Models of Proprioceptors. II. Structure and Function of the Golgi Tendon Organ. *Journal of Neurophysiology* [online]. 2006, **96**(4), 1789–1802. ISSN 0022-3077, 1522-1598. Available from: doi:[10.1152/jn.00869.2005](https://doi.org/10.1152/jn.00869.2005)
9. BARKER, D., HUNT, C.C., McINTYRE, A.K., 2012. *Muscle Receptors*, Handbook of Sensory Physiology. Springer Berlin Heidelberg. ISBN 10: 3540068910
10. JAMI, L. Golgi tendon organs in mammalian skeletal muscle: functional properties and central actions. *Physiological Reviews* [online]. 1992, **72**(3), 623–666. ISSN 0031-9333, 1522-1210. Available from: doi:[10.1152/physrev.1992.72.3.623](https://doi.org/10.1152/physrev.1992.72.3.623)
11. Proprioception. *Wikipedia*. Online. 2023. [Accessed 13 August 2023]. Available from: <https://en.wikipedia.org/w/index.php?title=Proprioception&oldid=1169720391> Page Version ID: 1169720391

12. NITATORI, Tohru. The fine structure of human Golgi tendon organs as studied by three-dimensional reconstruction. *Journal of Neurocytology* [online]. 1988, **17**(1), 27–41. ISSN 0300-4864, 1573-7381. Available from: doi:[10.1007/BF01735375](https://doi.org/10.1007/BF01735375)
13. SCHOULTZ, Ture W. a John E. SWETT. Ultrastructural organization of the sensory fibers innervating the Golgi tendon organ. *The Anatomical Record* [online]. 1974, **179**(2), 147–161. ISSN 0003-276X, 1097-0185. Available from: doi:[10.1002/ar.1091790202](https://doi.org/10.1002/ar.1091790202)
14. FUKAMI, Y a R S WILKINSON. Responses of isolated Golgi tendon organs of the cat. *The Journal of Physiology* [online]. 1977, **265**(3), 673–689. ISSN 00223751. Available from: doi:[10.1113/jphysiol.1977.sp011737](https://doi.org/10.1113/jphysiol.1977.sp011737)
15. CRAGO, P E, J C HOUK a W Z RYMER. Sampling of total muscle force by tendon organs. *Journal of Neurophysiology* [online]. 1982, **47**(6), 1069–1083. ISSN 0022-3077, 1522-1598. Available from: doi:[10.1152/jn.1982.47.6.1069](https://doi.org/10.1152/jn.1982.47.6.1069)
16. GREGORY, J E a U PROSKE. The responses of Golgi tendon organs to stimulation of different combinations of motor units. *The Journal of Physiology* [online]. 1979, **295**(1), 251–262. ISSN 00223751. Available from: doi:[10.1113/jphysiol.1979.sp012966](https://doi.org/10.1113/jphysiol.1979.sp012966)
17. GREGORY, J. E., D. L. MORGAN a U. PROSKE. Site of impulse initiation in tendon organs of cat soleus muscle. *Journal of Neurophysiology* [online]. 1985, **54**(6), 1383–1395. ISSN 0022-3077, 1522-1598. Available from: doi:[10.1152/jn.1985.54.6.1383](https://doi.org/10.1152/jn.1985.54.6.1383)
18. GREGORY, J. E. Relations between identified tendon organs and motor units in the medial gastrocnemius muscle of the cat. *Experimental Brain Research* [online]. 1990, **81**(3), 602–608. ISSN 0014-4819, 1432-1106. Available from: doi:[10.1007/BF02423510](https://doi.org/10.1007/BF02423510)
19. 9532 8001, 9532 8001, 9532 8001 and 9532 8011. Proprioception: Your Sixth Sense. 557. Online. 17 July 2014. [Accessed 15 August 2023]. Available from: <https://www.557.com.au/physiotherapy/proprioception-your-sixth-sense/>
20. VILÍMEK, Miloslav. *Musculotendon forces derived by different muscle models*. Acta of Bioengineering and Biomechanics. 2007, (92), 41-47.
21. Burrows, Malcolm, *The Neurobiology of an Insect Brain* (Oxford, 1996; online edn, Oxford Academic, 22 Mar. 2012), accessed 12 July 2023. <https://doi.org/10.1093/acprof:oso/9780198523444.001.0001>
22. CADOVA, Michala, Miloslav VILIMEK a Matej DANIEL. A comparative study of muscle force estimates using Huxley's and Hill's muscle model. *Computer Methods in Biomechanics and Biomedical Engineering* [online]. 2014, **17**(4), 311–317. ISSN 1025-5842, 1476-8259. Available from: doi:[10.1080/10255842.2012.683426](https://doi.org/10.1080/10255842.2012.683426)

23. KRYLOW, Andrew M. a Thomas G. SANDERCOCK. Dynamic force responses of muscle involving eccentric contraction. *Journal of Biomechanics* [online]. 1997, **30**(1), 27–33. ISSN 00219290. Available from: doi:[10.1016/S0021-9290\(96\)00097-8](https://doi.org/10.1016/S0021-9290(96)00097-8)
24. SACKS, Robert D. a Roland R. ROY. Architecture of the hind limb muscles of cats: Functional significance. *Journal of Morphology* [online]. 1982, **173**(2), 185–195. ISSN 0362-2525, 1097-4687. Available from: doi:[10.1002/jmor.1051730206](https://doi.org/10.1002/jmor.1051730206)
25. WILLIAMS, Ian a Timothy G. CONSTANDINOU. Computationally efficient modeling of proprioceptive signals in the upper limb for prostheses: a simulation study. *Frontiers in Neuroscience* [online]. 2014, **8** [vid. 2023-07-06]. ISSN 1662-453X. Available from: doi:[10.3389/fnins.2014.00181](https://doi.org/10.3389/fnins.2014.00181)
26. MILEUSNIC, Milana P., Ian E. BROWN, Ning LAN a Gerald E. LOEB. Mathematical Models of Proprioceptors. I. Control and Transduction in the Muscle Spindle. *Journal of Neurophysiology* [online]. 2006, **96**(4), 1772–1788. ISSN 0022-3077, 1522-1598. Available from: doi:[10.1152/jn.00868.2005](https://doi.org/10.1152/jn.00868.2005)
27. LIN, Chou-Ching K. a Patrick E. CRAGO. Neural and Mechanical Contributions to the Stretch Reflex: A Model Synthesis. *Annals of Biomedical Engineering* [online]. 2002, **30**(1), 54–67. ISSN 0090-6964. Available from: doi:[10.1114/1.1432692](https://doi.org/10.1114/1.1432692)
28. stretch reflex – Vyhledávání Google. Online. [Accessed 3 August 2023]. Available from: https://www.google.com/search?rlz=1C5CHFA_enCZ1064CZ1065&sxsrf=AB5stBgcs0v0E_Y74GGw4GWw0hi-qLH7Ow:1689455726480&q=stretch+reflex&tbm=isch&sa=X&ved=2ahUKEwio4cKD0ZGAAXWm_rsIHXXfC0wQ0pQJegQIChAB&biw=950&bih=912&dpr=1#imgsrc=7IsEM-Yf677kGM
29. MILEUSNIC, Milana P., Ian E. BROWN, Ning LAN a Gerald E. LOEB. Mathematical Models of Proprioceptors. I. Control and Transduction in the Muscle Spindle. *Journal of Neurophysiology* [online]. 2006, **96**(4), 1772–1788. ISSN 0022-3077, 1522-1598. Available from: doi:[10.1152/jn.00868.2005](https://doi.org/10.1152/jn.00868.2005)
30. KONVIČKOVÁ, Svatava, Jaroslav VALENTA a Tomáš MAREŠ. *Biomechanika svalstva člověka*. Praha: Nakladatelství ČVUT, 2007. ISBN 978-80-01-03911-3.
31. MYSLIVEČEK, Jaromír. *Základní fyziologické principy I*. Vyd. 2., přepřac. Praha: Nakladatelství ČVUT, 2007. ISBN 978-80-01-03599-3.
32. FABER, Herre, Arthur J. VAN SOEST a Dinant A. KISTEMAKER. Inverse dynamics of mechanical multibody systems: An improved algorithm that ensures consistency between

- kinematics and external forces. *PLOS ONE* [online]. 2018, **13**(9), e0204575. ISSN 1932-6203. Available from: doi:[10.1371/journal.pone.0204575](https://doi.org/10.1371/journal.pone.0204575)
33. THELEN, Darryl G., Frank C. ANDERSON a Scott L. DELP. Generating dynamic simulations of movement using computed muscle control. *Journal of Biomechanics* [online]. 2003, **36**(3), 321–328. ISSN 00219290. Available from: doi:[10.1016/S0021-9290\(02\)00432-3](https://doi.org/10.1016/S0021-9290(02)00432-3)
 34. DANIEL, RNDr Matej. *Mathematical simulation of the hip joint loading*. Dissertation thesis 2004, Faculty of Mechanical Engineering, CTU in Prague.
 35. YAMAGUCHI, Gary Tad. *Dynamic Modeling of Musculoskeletal Motion* [online]. Boston, MA: Springer US, 2001 [vid. 2023-07-20]. ISBN 978-0-387-28704-1. Available from: doi:[10.1007/978-0-387-28750-8](https://doi.org/10.1007/978-0-387-28750-8)
 36. NASR, Ali, Keaton A. INKOL, Sydney BELL a John MCPHEE. InverseMuscleNET: Alternative Machine Learning Solution to Static Optimization and Inverse Muscle Modeling. *Frontiers in Computational Neuroscience* [online]. 2021, **15**, 759489. ISSN 1662-5188. Available from: doi:[10.3389/fncom.2021.759489](https://doi.org/10.3389/fncom.2021.759489)
 37. ZATSIORSKY, Vladimir. The mass and inertia characteristics of the main segments of the human body. *Biomechanics*. 1983, s. 1152-1159,
 38. WINTER, David A. *Biomechanics and motor control of human movement*. 4th ed. Hoboken, N.J: Wiley, 2009. ISBN 978-0-470-39818-0.
 39. CHADWICK, Edward K., Dimitra BLANA, Robert F. KIRSCH a Antonie J. VAN DEN BOGERT. Real-Time Simulation of Three-Dimensional Shoulder Girdle and Arm Dynamics. *IEEE Transactions on Biomedical Engineering* [online]. 2014, **61**(7), 1947–1956. ISSN 0018-9294, 1558-2531. Available from: doi:[10.1109/TBME.2014.2309727](https://doi.org/10.1109/TBME.2014.2309727)
 40. YAKOVENKO, Sergiy a Arthur PROCHAZKA. Locomotor Control: From Spring-like Reactions of Muscles to Neural Prediction. In: Randall NELSON, ed. *The Somatosensory System* [online]. B.m.: CRC Press, 2001 [vid. 2023-08-01], *Frontiers in Neuroscience*. ISBN 978-0-8493-2336-2. Available from: doi:[10.1201/9781420038705.ch6](https://doi.org/10.1201/9781420038705.ch6)
 41. KISSANE, Roger W. P., James P. CHARLES, Robert W. BANKS a Karl T. BATES. Skeletal muscle function underpins muscle spindle abundance. *Proceedings of the Royal Society B: Biological Sciences* [online]. 2022, **289**(1976), 20220622. ISSN 0962-8452, 1471-2954. Available from: doi:[10.1098/rspb.2022.0622](https://doi.org/10.1098/rspb.2022.0622)
 42. BANKS RW. An allometric analysis of the number of muscle spindles in mammalian skeletal muscles. *J Anat.* 2006 Jun;208(6):753-68. doi: 10.1111/j.1469-7580.2006.00558.x. PMID: 16761976; PMCID: PMC2100235.

43. The ABC of EMG: A Practical Introduction to Kinesiological Electromyography [online]. Noraxon INC. USA: Peter Konrad, 2005 [cit. 2023-08-13]. Available from: https://hermanwallace.com/download/The_ABC_of_EMG_by_Peter_Konrad.pdf
44. DATE, Shota, Hiroshi KURUMADANI, Yuko NAKASHIMA, Yosuke ISHII, Akio UEDA, Kazuya KURAUCHI a Toru SUNAGAWA. Brachialis Muscle Activity Can Be Measured With Surface Electromyography: A Comparative Study Using Surface and Fine-Wire Electrodes. *Frontiers in Physiology* [online]. 2021, **12**, 809422. ISSN 1664-042X. Available from: doi:[10.3389/fphys.2021.809422](https://doi.org/10.3389/fphys.2021.809422)
45. CHAYTOR, Carla P., Davis FORMAN, Jeannette BYRNE, Angela LOUCKS-ATKINSON a Kevin E. POWER. Changes in muscle activity during the flexion and extension phases of arm cycling as an effect of power output are muscle-specific. *PeerJ* [online]. 2020, **8**, e9759. ISSN 2167-8359. Available from: doi:[10.7717/peerj.9759](https://doi.org/10.7717/peerj.9759)
46. GRAVES, Andrew E., Kurt W. KORNATZ a Roger M. ENOKA. Older Adults Use a Unique Strategy to Lift Inertial Loads With the Elbow Flexor Muscles. *Journal of Neurophysiology* [online]. 2000, **83**(4), 2030–2039. ISSN 0022-3077, 1522-1598. Available from: doi:[10.1152/jn.2000.83.4.2030](https://doi.org/10.1152/jn.2000.83.4.2030)
47. TSIKAROS, D., Baltzopoulos, V., & Bartlett, R. (1997). Inverse optimization: functional and physiological considerations related to the force-sharing problem. *Critical reviews in biomedical engineering*, 25(4-5), 371–40 <https://doi.org/10.1615/critrevbiomedeng.v25.i4-5.20>
48. RAIKOVA, Rositsa. A general approach for modelling and mathematical investigation of the human upper limb. *Journal of Biomechanics*. August 1992. Vol. 25, no. 8, p. 857–867. DOI [10.1016/0021-9290\(92\)90226-Q](https://doi.org/10.1016/0021-9290(92)90226-Q).
49. CROWNINSHIELD, Roy D. and BRAND, Richard A. A physiologically based criterion of muscle force prediction in locomotion. *Journal of Biomechanics*. January 1981. Vol. 14, no. 11, p. 793–801. DOI [10.1016/0021-9290\(81\)90035-X](https://doi.org/10.1016/0021-9290(81)90035-X).

9 Appendix

9.1 Appendix 1

https://github.com/jiribest/Master_thesis